Spin-Conserved and Spin-Flip Optical Excitations from the Bethe–Salpeter Equation Formalism

Enzo Monino and Pierre-François Loos*

Cite This: *J. Chem. Theory Comput.* 2021, 17, 2852−2867

Read Online

ACCESS | Metrics & More | Article Recommendations | SI Supporting Information

ABSTRACT: Like adiabatic time-dependent density-functional theory (TD-DFT), the Bethe−Salpeter equation (BSE) formalism of many-body perturbation theory, in its static approximation, is "blind" to double (and higher) excitations, which are ubiquitous, for example, in conjugated molecules like polyenes. Here, we apply the spin-flip *ansatz* (which considers the lowest triplet state as the reference configuration instead of the singlet ground state) to the BSE formalism in order to access, in particular, double excitations. The present scheme is based on a spin-unrestricted version of the *GW* approximation employed to compute the charged excitations and screened Coulomb potential required for the BSE calculations. Dynamical corrections to the static BSE optical excitations are taken into account via an unrestricted generalization of our recently developed (renormalized) perturbative treatment. The performance of the present spin-flip BSE formalism is illustrated by computing excited-state energies of the beryllium atom, the hydrogen molecule at various bond lengths, and cyclobutadiene in its rectangular and square-planar geometries.
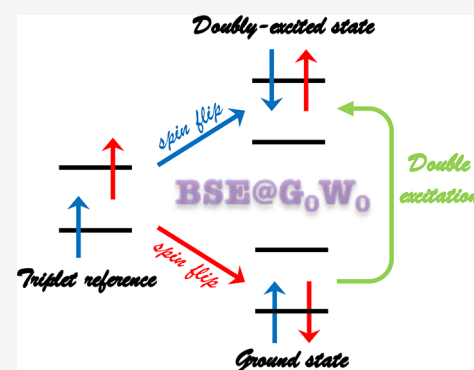
I. INTRODUCTION

Due to the ubiquitous influence of processes involving electronic excited states in physics, chemistry, and biology, their faithful description from first-principles has been one of the grand challenges faced by theoretical chemists since the dawn of computational chemistry. Accurately predicting ground- and excited-state energies (hence excitation energies) is particularly valuable in this context, and it has concentrated most of the efforts within the community. An armada of theoretical and computational methods has been developed to this end, each method being plagued by its own flaws.[1−12] The fact that none of these methods is successful in every chemical scenario has encouraged chemists to carry on the development of new excited-state methodologies, their main goal being to get the most accurate excitation energies (and properties) at the lowest possible computational cost in the most general context.[11]

Originally developed in the framework of nuclear physics[13] and popularized in condensed-matter physics,[14−16] one of the new emerging method in the computational chemistry landscape is the Bethe−Salpeter equation (BSE) formalism[10,13,17−22] from many-body perturbation theory,[23,24] which based on an underlying *GW* calculation to compute accurate charged excitations (i.e., ionization potentials and electron affinities) and the dynamically screened Coulomb potential,[25,26] is able to provide accurate optical (i.e., neutral) excitations for molecular systems at a rather modest computational cost.[10,22,27−44] Most of the BSE implementations rely on the so-called static approximation,[22,39,41,45] which approximates the dynamical (i.e., frequency-dependent) BSE kernel by its static limit. Like adiabatic time-dependent density-functional theory

(TD-DFT),[46−49] the static BSE formalism is plagued by the lack of double (and higher) excitations, which are, for example, ubiquitous in conjugated molecules like polyenes[50−57] or the ground state of open-shell molecules.[58−60] Indeed, both adiabatic TD-DFT[61−65] and static BSE[66−70] can only access (singlet and triplet) single excitations with respect to the reference determinant usually taken as the closed-shell singlet ground state. Double excitations are even challenging for state-of-the-art methods,[11,57,71−73] like the approximate third-order coupled-cluster (CC3) method[74,75] or equation-of-motion coupled-cluster with singles, doubles, and triples (EOM-CCSDT).[76−79]

One way to access double excitations is via the spin-flip formalism established by Krylov in 2001,[80−82] with earlier attempts by Bethe,[83] as well as Shibuya and McKoy.[84] The idea behind the spin-flip *ansatz* is rather simple: instead of considering the singlet ground state as reference, the reference configuration is taken as the lowest triplet state. In such a way, one can access the singlet ground state and the singlet doubly excited state via a spin-flip deexcitation and excitation (respectively), the difference of these two excitation energies providing an estimate of the double excitation. We refer the

interested reader to refs 4, 12, and 85 for detailed reviews on spin-flip methods. Note that a similar idea has been exploited by the group of Yang to access double excitations in the context of the particle–particle random-phase approximation.[86−91]

One obvious issue of spin-flip methods is that not all double excitations are accessible in such a way. Moreover, spin-flip methods are usually hampered by spin contamination[12] (i.e., artificial mixing with configurations of different spin multiplicities) due to spin incompleteness of the configuration interaction expansion as well as the possible spin contamination of the reference configuration.[92] This issue can be alleviated by increasing the excitation order at a significant cost or by selectively complementing the spin-incomplete configuration set with the missing configurations.[93−100]

Nowadays, spin-flip techniques are widely available for many types of methods such as equation-of-motion coupled cluster (EOM-CC),[80,101−104] configuration interaction (CI),[81,82,94,105,106] TD-DFT,[97,99,107−109] the algebraic-diagrammatic construction (ADC) scheme,[110,111] and others[112−115] with successful applications in bond breaking processes,[116] radical chemistry,[117−124] and photochemistry in general[111,125−127] to mention a few.

Here we apply the spin-flip technique to the BSE formalism in order to access, in particular, double excitations,[70] but not only. The present BSE calculations are based on the spin-unrestricted version of both *GW* (Section II) and BSE (Section III). To the best of our knowledge, the present study is the first to apply the spin-flip formalism to the BSE method. Moreover, we also go beyond the static approximation by taking into account dynamical effects (Section III.B) via an unrestricted generalization of our recently developed (renormalized) perturbative correction, which builds on the seminal work of Strinati,[15,17,128] Romaniello and collaborators,[67,68] and Rohlfing and co-workers.[129−133] We also discuss the computation of oscillator strengths (Section III.C) and the expectation value of the spin operator $\langle \hat{S}^2 \rangle$ as a diagnostic of the spin contamination for both ground and excited states (Section III.D). Computational details are reported in Section IV and our results for the beryllium atom Be (Section VV.A), the hydrogen molecule H_2 (Section V.B), and cyclobutadiene C_4H_4 (Section V.C) are discussed in Section V. Finally, we draw our conclusions in Section VI. Unless otherwise stated, atomic units are used.

II. UNRESTRICTED *GW* FORMALISM

Let us consider an electronic system consisting of $n = n_\uparrow + n_\downarrow$ electrons (where $n_\uparrow$ and $n_\downarrow$ are the number of spin-up and spin-down electrons, respectively) and N one-electron basis functions. The number of spin-up and spin-down occupied orbitals are $O_\uparrow = n_\uparrow$ and $O_\downarrow = n_\downarrow$, respectively, and, assuming the absence of linear dependencies in the one-electron basis set, there is $V_\uparrow = N - O_\uparrow$ and $V_\downarrow = N - O_\downarrow$ spin-up and spin-down virtual (i.e., unoccupied) orbitals. The number of spin-conserved (sc) single excitations is then $S^{sc} = S^{sc}_{\uparrow\uparrow} + S^{sc}_{\downarrow\downarrow} = O_\uparrow V_\uparrow + O_\downarrow V_\downarrow$, while the number of spin-flip (sf) excitations is $S^{sf} = S^{sf}_{\uparrow\downarrow} + S^{sf}_{\downarrow\uparrow} = O_\uparrow V_\downarrow + O_\downarrow V_\uparrow$. Let us denote as $\phi_{p_\sigma}(\mathbf{r})$ the pth spatial orbital associated with the spin-σ electrons (where $\sigma = \uparrow$ or $\downarrow$) and ε_{p_σ} its one-electron energy. It is important to understand that, in a spin-conserved excitation, the hole orbital ϕ_{i_σ} and particle orbital ϕ_{a_σ} have the same spin σ. In a spin-flip excitation, the hole and particle states, ϕ_{i_σ} and $\phi_{a_{\bar\sigma}}$, have opposite spins, σ and $\bar\sigma$. We assume real quantities throughout this manuscript, i

and j are occupied orbitals, a and b are unoccupied orbitals, p, q, r, and s indicate arbitrary orbitals, and m labels single excitations. Moreover, we consider systems with collinear spins and a spin-independent Hamiltonian without contributions such as a spin–orbit interaction.

II.A. The Dynamical Screening. The pillar of Green's function many-body perturbation theory is the (time-ordered) one-body Green's function, which has poles at the charged excitations (i.e., ionization potentials and electron affinities) of the system.[66] The spin-σ component of the one-body Green's function reads[45,66]

$$G^\sigma(\mathbf{r}_1, \mathbf{r}_2; \omega) = \sum_i \frac{\phi_{i_\sigma}(\mathbf{r}_1)\phi_{i_\sigma}(\mathbf{r}_2)}{\omega - \varepsilon_{i_\sigma} - i\eta} + \sum_a \frac{\phi_{a_\sigma}(\mathbf{r}_1)\phi_{a_\sigma}(\mathbf{r}_2)}{\omega - \varepsilon_{a_\sigma} + i\eta} \tag{1}$$

where η is a positive infinitesimal. As readily seen in eq 1, the Green's function can be evaluated at different levels of theory depending on the choice of orbitals and energies, ϕ_{p_σ} and ε_{p_σ}. For example, G^σ_{KS} is the independent-particle Green's function built with Kohn–Sham (KS) orbitals $\phi^{KS}_{p_\sigma}(\mathbf{r})$ and one-electron energies $\varepsilon^{KS}_{p_\sigma}$.[134−136] Within self-consistent schemes, these quantities can be replaced by quasiparticle energies and orbitals evaluated within the *GW* approximation (see below).[25,26]

Based on the spin-up and spin-down components of G defined in eq 1, one can easily compute the noninteracting polarizability (which is a sum over spins)

$$\chi_0(\mathbf{r}_1, \mathbf{r}_2; \omega)$$
$$= -\frac{i}{2\pi} \sum_\sigma \int G^\sigma(\mathbf{r}_1, \mathbf{r}_2; \omega + \omega') G^\sigma(\mathbf{r}_1, \mathbf{r}_2; \omega') \, d\omega' \tag{2}$$

and subsequently the dielectric function

$$\varepsilon(\mathbf{r}_1, \mathbf{r}_2; \omega) = \delta(\mathbf{r}_1 - \mathbf{r}_2) - \int \frac{\chi_0(\mathbf{r}_1, \mathbf{r}_3; \omega)}{|\mathbf{r}_2 - \mathbf{r}_3|} \, d\mathbf{r}_3 \tag{3}$$

where $\delta(\mathbf{r})$ is the Dirac delta function. Based on this latter ingredient, one can access the dynamically screened Coulomb potential

$$W(\mathbf{r}_1, \mathbf{r}_2; \omega) = \int \frac{\varepsilon^{-1}(\mathbf{r}_1, \mathbf{r}_3; \omega)}{|\mathbf{r}_2 - \mathbf{r}_3|} \, d\mathbf{r}_3 \tag{4}$$

which is naturally spin independent as the bare Coulomb interaction $|\mathbf{r}_1 - \mathbf{r}_2|^{-1}$ does not depend on spin coordinates.

Within the *GW* formalism,[23,25,26] the dynamical screening is computed at the random-phase approximation (RPA) level by considering only the manifold of the spin-conserved neutral excitations. In the orbital basis, the spectral representation of W is

$$W_{p_\sigma q_\sigma, r_{\sigma'} s_{\sigma'}}(\omega) = (p_\sigma q_\sigma | r_{\sigma'} s_{\sigma'}) + \sum_m (p_\sigma q_\sigma | m)(r_{\sigma'} s_{\sigma'} | m)$$
$$\times \left[\frac{1}{\omega - \Omega^{sc,RPA}_m + i\eta} - \frac{1}{\omega + \Omega^{sc,RPA}_m - i\eta} \right] \tag{5}$$

where the bare two-electron integrals are[137]

$$(p_\sigma q_\tau | r_{\sigma'} s_{\tau'}) = \iint \frac{\phi_{p_\sigma}(\mathbf{r}_1)\phi_{q_\tau}(\mathbf{r}_1)\phi_{r_{\sigma'}}(\mathbf{r}_2)\phi_{s_{\tau'}}(\mathbf{r}_2)}{|\mathbf{r}_1 - \mathbf{r}_2|} \, d\mathbf{r}_1 \, d\mathbf{r}_2 \tag{6}$$

and the screened two-electron integrals (or spectral weights) are explicitly given by

$$(p_\sigma q_\sigma | m) = \sum_{ia\sigma'} (p_\sigma q_\sigma | i_{\sigma'} a_{\sigma'}) (\mathbf{X}_m^{sc,RPA} + \mathbf{Y}_m^{sc,RPA})_{i_{\sigma'} a_{\sigma'}} \quad (7)$$

In eqs 5 and 7, the spin-conserved RPA neutral excitations $\Omega_m^{sc,RPA}$ and their corresponding eigenvectors, $\mathbf{X}_m^{sc,RPA}$ and $\mathbf{Y}_m^{sc,RPA}$, are obtained by solving a linear response system of the form

$$\begin{pmatrix} \mathbf{A} & \mathbf{B} \\ -\mathbf{B} & -\mathbf{A} \end{pmatrix} \cdot \begin{pmatrix} \mathbf{X}_m \\ \mathbf{Y}_m \end{pmatrix} = \Omega_m \begin{pmatrix} \mathbf{X}_m \\ \mathbf{Y}_m \end{pmatrix} \quad (8)$$

where the expressions of the matrix elements of $\mathbf{A}$ and $\mathbf{B}$ are specific of the method and of the spin manifold. The spin structure of these matrices, though, is general

$$\mathbf{A}^{sc} = \begin{pmatrix} \mathbf{A}^{\uparrow\uparrow,\uparrow\uparrow} & \mathbf{A}^{\uparrow\uparrow,\downarrow\downarrow} \\ \mathbf{A}^{\downarrow\downarrow,\uparrow\uparrow} & \mathbf{A}^{\downarrow\downarrow,\downarrow\downarrow} \end{pmatrix} \qquad \mathbf{B}^{sc} = \begin{pmatrix} \mathbf{B}^{\uparrow\uparrow,\uparrow\uparrow} & \mathbf{B}^{\uparrow\uparrow,\downarrow\downarrow} \\ \mathbf{B}^{\downarrow\downarrow,\uparrow\uparrow} & \mathbf{B}^{\downarrow\downarrow,\downarrow\downarrow} \end{pmatrix} \quad (9a)$$

$$\mathbf{A}^{sf} = \begin{pmatrix} \mathbf{A}^{\uparrow\downarrow,\uparrow\downarrow} & \mathbf{0} \\ \mathbf{0} & \mathbf{A}^{\downarrow\uparrow,\downarrow\uparrow} \end{pmatrix} \qquad \mathbf{B}^{sf} = \begin{pmatrix} \mathbf{0} & \mathbf{B}^{\uparrow\downarrow,\downarrow\uparrow} \\ \mathbf{B}^{\downarrow\uparrow,\uparrow\downarrow} & \mathbf{0} \end{pmatrix} \quad (9b)$$

In the absence of instabilities, the linear eigenvalue problem (8) has particle−hole symmetry which means that the eigenvalues are obtained by pairs $\pm\Omega_m$. In such a case, $(\mathbf{A} - \mathbf{B})^{1/2}$ is positive definite, and eq 8 can be recast as a Hermitian problem of half its original dimension

$$(\mathbf{A} - \mathbf{B})^{1/2} \cdot (\mathbf{A} + \mathbf{B}) \cdot (\mathbf{A} - \mathbf{B})^{1/2} \cdot \mathbf{Z} = \Omega^2 \cdot \mathbf{Z} \quad (10)$$

where the excitation amplitudes are

$$\mathbf{X} + \mathbf{Y} = \Omega^{-1/2} \cdot (\mathbf{A} - \mathbf{B})^{1/2} \cdot \mathbf{Z} \quad (11)$$

Within the Tamm−Dancoff approximation (TDA), the coupling terms between the resonant and antiresonant parts, $\mathbf{A}$ and $-\mathbf{A}$, are neglected, which consists in setting $\mathbf{B} = \mathbf{0}$. In such a case, eq 8 reduces to a straightforward Hermitian problem of the following form:

$$\mathbf{A} \cdot \mathbf{X}_m = \Omega_m \mathbf{X}_m \quad (12)$$

Note that, for spin-flip excitations, it is quite common to enforce the TDA, especially when one considers a triplet reference as the first "excited-state" is usually the ground state of the closed-shell system (hence, corresponding to a negative excitation energy or deexcitation).

At the RPA level, the matrix elements of $\mathbf{A}$ and $\mathbf{B}$ are

$$A_{i_\sigma a_\tau, j_{\sigma'} b_{\tau'}}^{RPA} = \delta_{ij}\delta_{ab}\delta_{\sigma\sigma'}\delta_{\tau\tau'}(\varepsilon_{a_\tau} - \varepsilon_{i_\sigma}) + (i_\sigma a_\tau | b_{\tau'} j_{\sigma'}) \quad (13a)$$

$$B_{i_\sigma a_\tau, j_{\sigma'} b_{\tau'}}^{RPA} = (i_\sigma a_\tau | j_{\sigma'} b_{\tau'}) \quad (13b)$$

from which we obtain the following expressions:

$$A_{i_\sigma a_\sigma, j_{\sigma'} b_{\sigma'}}^{sc,RPA} = \delta_{ij}\delta_{ab}\delta_{\sigma\sigma'}(\varepsilon_{a_\sigma} - \varepsilon_{i_\sigma}) + (i_\sigma a_\sigma | b_{\sigma'} j_{\sigma'}) \quad (14a)$$

$$B_{i_\sigma a_\sigma, j_{\sigma'} b_{\sigma'}}^{sc,RPA} = (i_\sigma a_\sigma | j_{\sigma'} b_{\sigma'}) \quad (14b)$$

for the spin-conserved excitations and

$$A_{i_\sigma a_{\bar\sigma}, j_\sigma b_{\bar\sigma}}^{sf,RPA} = \delta_{ij}\delta_{ab}(\varepsilon_{a_{\bar\sigma}} - \varepsilon_{i_\sigma}) \quad (15a)$$

$$B_{i_\sigma a_{\bar\sigma}, j_{\bar\sigma} b_\sigma}^{sf,RPA} = 0 \quad (15b)$$

for the spin-flip excitations.

II.B. The *GW* Self-Energy. Within the acclaimed *GW* approximation,[25,26] the exchange-correlation (xc) part of the self-energy

$$\Sigma^{xc,\sigma}(\mathbf{r}_1, \mathbf{r}_2; \omega) = \Sigma^{x,\sigma}(\mathbf{r}_1, \mathbf{r}_2) + \Sigma^{c,\sigma}(\mathbf{r}_1, \mathbf{r}_2; \omega)$$

$$= \frac{i}{2\pi} \int G^\sigma(\mathbf{r}_1, \mathbf{r}_2; \omega + \omega') W(\mathbf{r}_1, \mathbf{r}_2; \omega') e^{i\eta\omega'} \, d\omega' \quad (16)$$

is, like the one-body Green's function, spin-diagonal, and its spectral representation reads

$$\Sigma_{p_\sigma q_\sigma}^{x} = -\sum_i (p_\sigma i_\sigma | i_\sigma q_\sigma) \quad (17a)$$

$$\Sigma_{p_\sigma q_\sigma}^{c}(\omega) = \sum_{im} \frac{(p_\sigma i_\sigma | m)(q_\sigma i_\sigma | m)}{\omega - \varepsilon_{i_\sigma} + \Omega_m^{sc,RPA} - i\eta}$$

$$+ \sum_{am} \frac{(p_\sigma a_\sigma | m)(q_\sigma a_\sigma | m)}{\omega - \varepsilon_{a_\sigma} - \Omega_m^{sc,RPA} + i\eta} \quad (17b)$$

where the self-energy has been split in its exchange (x) and correlation (c) contributions. The Dyson equation linking the Green's function and the self-energy holds separately for each spin component

$$[G^\sigma(\mathbf{r}_1, \mathbf{r}_2; \omega)]^{-1} = [G_{KS}^\sigma(\mathbf{r}_1, \mathbf{r}_2; \omega)]^{-1}$$

$$+ \Sigma^{xc,\sigma}(\mathbf{r}_1, \mathbf{r}_2; \omega) - v^{xc}(\mathbf{r}_1)\delta(\mathbf{r}_1 - \mathbf{r}_2) \quad (18)$$

where $v^{xc}(\mathbf{r})$ is the KS (local) exchange-correlation potential. The target quantities here are the quasiparticle energies $\varepsilon_{p_\sigma}^{GW}$, i.e., the poles of G [see eq 1], which correspond to well-defined addition/removal energies (unlike the KS orbital energies). Because the exchange-correlation part of the self-energy is, itself, constructed with the Green's function (see eq 16), the present process is, by nature, self-consistent. The same comment applies to the dynamically screened Coulomb potential W entering the definition of Σ^{xc} [see eq 16], which is also constructed from G (see eqs 2, 3, and 4).

II.C. Level of Self-Consistency. This is where *GW* schemes differ. In its simplest perturbative (i.e., one-shot) version, known as $G_0 W_0$,[138−146] a single iteration is performed, and the quasiparticle energies $\varepsilon_{p_\sigma}^{GW}$ are obtained by solving the frequency-dependent quasiparticle equation

$$\omega = \varepsilon_{p\sigma}^{KS} + \Sigma_{p_\sigma}^{xc}(\omega) - V_{p_\sigma}^{xc} \quad (19)$$

where $\Sigma_{p_\sigma}^{xc}(\omega) \equiv \Sigma_{p_\sigma p_\sigma}^{xc}(\omega)$ and its offspring quantities have been constructed at the KS level, and

$$V_{p_\sigma}^{xc} = \int \phi_{p_\sigma}(\mathbf{r}) v^{xc}(\mathbf{r}) \phi_{p_\sigma}(\mathbf{r}) \, d\mathbf{r} \quad (20)$$

Because, from a practical point of view, one is usually interested by the so-called quasiparticle solution (or peak), the quasiparticle eq 19 is often linearized around $\omega = \varepsilon_{p_\sigma}^{KS}$, yielding

$$\varepsilon_{p_\sigma}^{GW} = \varepsilon_{p_\sigma}^{KS} + Z_{p_\sigma} \left[\Sigma_{p_\sigma}^{xc}(\varepsilon_{p_\sigma}^{KS}) - V_{p_\sigma}^{xc} \right] \quad (21)$$

where

$$Z_{p_\sigma} = \left[1 - \left. \frac{\partial \Sigma_{p_\sigma}^{xc}(\omega)}{\partial \omega} \right|_{\omega = \varepsilon_{p_\sigma}^{KS}} \right]^{-1}$$

(22)

is a renormalization factor (with $0 \leq Z_{p_\sigma} \leq 1$) which also represents the spectral weight of the quasiparticle solution. In addition to the principal quasiparticle peak, which, in a well-behaved case, contains most of the spectral weight, the frequency-dependent quasiparticle eq 19 generates a finite number of satellite resonances with smaller weights.[147]

Within the "eigenvalue" self-consistent GW scheme (known as evGW),[40,140,146,148−150] several iterations are performed during which only the one-electron energies entering the definition of the Green's function (see eq 1) are updated by the quasiparticle energies obtained at the previous iteration (the corresponding orbitals remain evaluated at the KS level).

Finally, within the quasiparticle self-consistent GW (qsGW) scheme,[151−155] both the one-electron energies and the orbitals are updated until convergence is reached. These are obtained via the diagonalization of an effective Fock matrix, which includes explicitly a frequency-independent Hermitian self-energy defined as

$$\tilde{\Sigma}_{p_\sigma q_\sigma}^{xc} = \frac{1}{2} \left[\Sigma_{p_\sigma q_\sigma}^{xc}(\varepsilon_{p_\sigma}) + \Sigma_{q_\sigma p_\sigma}^{xc}(\varepsilon_{p_\sigma}) \right]$$

(23)

III. UNRESTRICTED BETHE−SALPETER EQUATION FORMALISM

Like its TD-DFT cousin,[3,46−48] the BSE formalism[13,17−21] deals with the calculation of (neutral) optical excitations as measured by absorption spectroscopy.[27−40] Using the BSE formalism, one can access the spin-conserved and spin-flip excitations. In a nutshell, BSE builds on top of a GW calculation by adding up excitonic effects (i.e., the electron−hole binding energy) to the GW fundamental gap, which is itself a corrected version of the KS gap. The purpose of the underlying GW calculation is to provide quasiparticle energies and a dynamically screened Coulomb potential that are used to build the BSE Hamiltonian from which the vertical excitations of the system are extracted.

III.A. Static Approximation. Within the so-called static approximation of BSE, the Dyson equation that links the generalized four-point susceptibility $L^{\sigma\sigma'}(\mathbf{r}_1,\mathbf{r}_2;\mathbf{r}'_1,\mathbf{r}'_2;\omega)$ and the BSE kernel $\Xi^{\sigma\sigma'}(\mathbf{r}_3,\mathbf{r}_5;\mathbf{r}_4,\mathbf{r}_6)$ is[45,66]

$$L^{\sigma\sigma'}(\mathbf{r}_1, \mathbf{r}_2; \mathbf{r}'_1, \mathbf{r}'_2; \omega) = L_0^{\sigma\sigma'}(\mathbf{r}_1, \mathbf{r}_2; \mathbf{r}'_1, \mathbf{r}'_2; \omega)$$
$$+ \int L_0^{\sigma\sigma'}(\mathbf{r}_1, \mathbf{r}_4; \mathbf{r}'_1, \mathbf{r}_3; \omega) \Xi^{\sigma\sigma'}(\mathbf{r}_3, \mathbf{r}_5; \mathbf{r}_4, \mathbf{r}_6)$$
$$\times L^{\sigma\sigma'}(\mathbf{r}_6, \mathbf{r}_2; \mathbf{r}_5, \mathbf{r}'_2; \omega) \, d\mathbf{r}_3 \, d\mathbf{r}_4 \, d\mathbf{r}_5 \, d\mathbf{r}_6$$

(24)

where

$$L_0^{\sigma\sigma'}(\mathbf{r}_1, \mathbf{r}_2; \mathbf{r}'_1, \mathbf{r}'_2; \omega)$$
$$= \frac{1}{2\pi} \int G^\sigma(\mathbf{r}_1, \mathbf{r}'_2; \omega + \omega') G^\sigma(\mathbf{r}'_1, \mathbf{r}_2; \omega') \, d\omega'$$

(25)

is the noninteracting analog of the two-particle correlation function L.

Within the GW approximation, the static BSE kernel is

$$i\Xi^{\sigma\sigma'}(\mathbf{r}_3, \mathbf{r}_5; \mathbf{r}_4, \mathbf{r}_6) = \frac{\delta(\mathbf{r}_3 - \mathbf{r}_4)\delta(\mathbf{r}_5 - \mathbf{r}_6)}{|\mathbf{r}_3 - \mathbf{r}_6|}$$
$$- \delta_{\sigma\sigma'} W(\mathbf{r}_3, \mathbf{r}_4; \omega = 0)\delta(\mathbf{r}_3 - \mathbf{r}_6)\delta(\mathbf{r}_4 - \mathbf{r}_6)$$

(26)

where, as usual, we have not considered the higher-order terms in W by neglecting the derivative $\partial W/\partial G$.[15,17,128,156]

As readily seen in eq 26, the static approximation consists in neglecting the frequency dependence of the dynamically screened Coulomb potential. In this case, the spin-conserved and spin-flip BSE optical excitations are obtained by solving the usual Casida-like linear response (eigen)problem:

$$\begin{pmatrix} \mathbf{A}^{BSE} & \mathbf{B}^{BSE} \\ -\mathbf{B}^{BSE} & -\mathbf{A}^{BSE} \end{pmatrix} \cdot \begin{pmatrix} \mathbf{X}_m^{BSE} \\ \mathbf{Y}_m^{BSE} \end{pmatrix} = \Omega_m^{BSE} \begin{pmatrix} \mathbf{X}_m^{BSE} \\ \mathbf{Y}_m^{BSE} \end{pmatrix}$$

(27)

Defining the elements of the static screening as $W_{p_\sigma q_\sigma, r_{\sigma'} s_{\sigma'}}^{stat} = W_{p_\sigma q_\sigma, r_{\sigma'} s_{\sigma'}}(\omega = 0)$, the general expressions of the BSE matrix elements are

$$A_{i_\sigma a_\tau, j_\sigma b_{\tau'}}^{BSE} = A_{i_\sigma a_\tau, j_\sigma b_{\tau'}}^{RPA} - \delta_{\sigma\sigma'} W_{i_\sigma j_{\sigma'}, b_{\tau'} a_\tau}^{stat}$$

(28a)

$$B_{i_\sigma a_\tau, j_\sigma b_{\tau'}}^{BSE} = B_{i_\sigma a_\tau, j_\sigma b_{\tau'}}^{RPA} - \delta_{\sigma\sigma'} W_{i_\sigma b_{\tau'}, j_\sigma a_\tau}^{stat}$$

(28b)

from which we obtain the following expressions for the spin-conserved and spin-flip BSE excitations:

$$A_{i_\sigma a_\sigma, j_\sigma b_{\sigma'}}^{sc,BSE} = A_{i_\sigma a_\sigma, j_\sigma b_{\sigma'}}^{sc,RPA} - \delta_{\sigma\sigma'} W_{i_\sigma j_{\sigma'}, b_\sigma a_\sigma}^{stat}$$

(29a)

$$B_{i_\sigma a_\sigma, j_\sigma b_{\sigma'}}^{sc,BSE} = B_{i_\sigma a_\sigma, j_\sigma b_{\sigma'}}^{sc,RPA} - \delta_{\sigma\sigma'} W_{i_\sigma b_{\sigma'}, j_\sigma a_\sigma}^{stat}$$

(29b)

$$A_{i_\sigma a_{\bar\sigma}, j_\sigma b_{\bar\sigma}}^{sf,BSE} = A_{i_\sigma a_{\bar\sigma}, j_\sigma b_{\bar\sigma}}^{sf,RPA} - W_{i_\sigma j_\sigma, b_{\bar\sigma} a_{\bar\sigma}}^{stat}$$

(29c)

$$B_{i_\sigma a_{\bar\sigma}, j_\sigma b_{\bar\sigma}}^{sf,BSE} = - W_{i_\sigma b_\sigma, j_\sigma a_{\bar\sigma}}^{stat}$$

(29d)

At this stage, it is of particular interest to discuss the form of the spin-flip matrix elements defined in eqs 29c and 29d. As readily seen from eq 15a, at the RPA level, the spin-flip excitations are given by the difference of one-electron energies, hence missing out on key exchange and correlation effects. This is also the case at the TD-DFT level when one relies on (semi)local functionals. This explains why most of the spin-flip TD-DFT calculations are performed with global hybrid functionals containing a substantial amount of Hartree−Fock exchange as only the exact exchange integral of the form $(i_\sigma j_\sigma|b_{\bar\sigma} a_{\bar\sigma})$ survive spin-symmetry requirements. At the BSE level, these matrix elements are, of course, also present thanks to the contribution of $W_{i_\sigma j_\sigma, b_{\bar\sigma} a_{\bar\sigma}}^{stat}$ as evidenced in eq 5, but it also includes correlation effects.

III.B. Dynamical Correction. In order to go beyond the ubiquitous static approximation of BSE[17,59,67,68,129−131,133,157−162] (which is somehow similar to the adiabatic approximation of TD-DFT[50,51,58,59,63,64,163]), we have recently implemented, following Strinati's seminal work[15,17,128] (see also the work of Romaniello et al.[67] and Sangalli et al.[68]), a renormalized first-order perturbative correction in order to take into consideration the dynamical nature of the screened Coulomb potential W.[69,70] This dynamical correction to the static BSE kernel (dubbed as dBSE in the following) does permit one to recover additional relaxation effects coming from higher excitations.

Our implementation follows closely the work of Rohlfing and co-workers[129−132] in which they computed the dynamical correction in the TDA and plasmon−pole approximation. However, our scheme goes beyond the plasmon−pole approximation as the spectral representation of the dynamically screened Coulomb potential is computed exactly at the RPA level consistently with the underlying *GW* calculation:

$$\tilde{W}_{p_\sigma q_\sigma, r_{\sigma'} s_{\sigma'}}(\omega) = (p_\sigma q_\sigma | r_{\sigma'} s_{\sigma'}) + \sum_m (p_\sigma q_\sigma | m)(r_{\sigma'} s_{\sigma'} | m)$$

$$\times \left[\frac{1}{\omega - (\varepsilon^{GW}_{s_{\sigma'}} - \varepsilon^{GW}_{q_\sigma}) - \Omega^{sc,RPA}_m + i\eta} \right.$$

$$\left. + \frac{1}{\omega - (\varepsilon^{GW}_{r_{\sigma'}} - \varepsilon^{GW}_{p_\sigma}) - \Omega^{sc,RPA}_m + i\eta} \right] \quad (30)$$

The dBSE nonlinear response problem is

$$\begin{pmatrix} \mathbf{A}^{dBSE}(\Omega^{dBSE}_m) & \mathbf{B}^{dBSE}(\Omega^{dBSE}_m) \\ -\mathbf{B}^{dBSE}(-\Omega^{dBSE}_m) & -\mathbf{A}^{dBSE}(-\Omega^{dBSE}_m) \end{pmatrix} \cdot \begin{pmatrix} \mathbf{X}^{dBSE}_m \\ \mathbf{Y}^{dBSE}_m \end{pmatrix}$$

$$= \Omega^{dBSE}_m \begin{pmatrix} \mathbf{X}^{dBSE}_m \\ \mathbf{Y}^{dBSE}_m \end{pmatrix} \quad (31)$$

where the dynamical matrices are generally defined as

$$A^{dBSE}_{i_\sigma a_\tau, j_{\sigma'} b_{\tau'}}(\omega) = A^{RPA}_{i_\sigma a_\tau, j_{\sigma'} b_{\tau'}} - \delta_{\sigma\sigma'} \tilde{W}_{i_\sigma j_{\sigma'}, b_{\tau'} a_\tau}(\omega) \quad (32a)$$

$$B^{dBSE}_{i_\sigma a_\tau, j_{\sigma'} b_{\tau'}}(\omega) = B^{RPA}_{i_\sigma a_\tau, j_{\sigma'} b_{\tau'}} - \delta_{\sigma\sigma'} \tilde{W}_{i_\sigma b_{\tau'}, j_{\sigma'} a_\tau}(\omega) \quad (32b)$$

from which one can easily obtained the matrix elements for the spin-conserved and spin-flip manifolds similar to eqs 29a, 29b, 29c, and 29d. Following Rayleigh−Schrödinger perturbation theory, we then decompose the nonlinear eigenproblem (31) as a zeroth-order static (i.e., linear) reference and a first-order dynamic (i.e., nonlinear) perturbation such that

$$\begin{pmatrix} \mathbf{A}^{dBSE}(\omega) & \mathbf{B}^{dBSE}(\omega) \\ -\mathbf{B}^{dBSE}(-\omega) & -\mathbf{A}^{dBSE}(-\omega) \end{pmatrix}$$

$$= \begin{pmatrix} \mathbf{A}^{(0)} & \mathbf{B}^{(0)} \\ -\mathbf{B}^{(0)} & -\mathbf{A}^{(0)} \end{pmatrix} + \begin{pmatrix} \mathbf{A}^{(1)}(\omega) & \mathbf{B}^{(1)}(\omega) \\ -\mathbf{B}^{(1)}(-\omega) & -\mathbf{A}^{(1)}(-\omega) \end{pmatrix} \quad (33)$$

with

$$A^{(0)}_{i_\sigma a_\tau, j_{\sigma'} b_{\tau'}} = A^{BSE}_{i_\sigma a_\tau, j_{\sigma'} b_{\tau'}} \quad (34a)$$

$$B^{(0)}_{i_\sigma a_\tau, j_{\sigma'} b_{\tau'}} = B^{BSE}_{i_\sigma a_\tau, j_{\sigma'} b_{\tau'}} \quad (34b)$$

and

$$A^{(1)}_{i_\sigma a_\tau, j_{\sigma'} b_{\tau'}}(\omega) = -\delta_{\sigma\sigma'} \tilde{W}_{i_\sigma j_{\sigma'}, b_{\tau'} a_\tau}(\omega) + \delta_{\sigma\sigma'} W^{stat}_{i_\sigma j_{\sigma'}, b_{\tau'} a_\tau} \quad (35a)$$

$$B^{(1)}_{i_\sigma a_\tau, j_{\sigma'} b_{\tau'}}(\omega) = -\delta_{\sigma\sigma'} \tilde{W}_{i_\sigma b_{\tau'}, j_{\sigma'} a_\tau}(\omega) + \delta_{\sigma\sigma'} W^{stat}_{i_\sigma b_{\tau'}, j_{\sigma'} a_\tau} \quad (35b)$$

The dBSE excitation energies are then obtained via

$$\Omega^{dBSE}_m = \Omega^{BSE}_m + \zeta_m \Omega^{(1)}_m \quad (36)$$

where $\Omega^{BSE}_m \equiv \Omega^{(0)}_m$ are the static (zeroth-order) BSE excitation energies obtained by solving eq 27, and

$$\Omega^{(1)}_m = (\mathbf{X}^{BSE}_m)^T \cdot \mathbf{A}^{(1)}(\Omega^{BSE}_m) \cdot \mathbf{X}^{BSE}_m \quad (37)$$

are first-order corrections (with $\mathbf{X}^{BSE}_m \equiv \mathbf{X}^{(0)}_m$) obtained within the dynamical TDA (dTDA) with the renormalization factor

$$\zeta_m = \left[1 - (\mathbf{X}^{BSE}_m)^T \cdot \left. \frac{\partial \mathbf{A}^{(1)}(\omega)}{\partial \omega} \right|_{\omega = \Omega^{BSE}_m} \cdot \mathbf{X}^{BSE}_m \right]^{-1} \quad (38)$$

which, unlike the *GW* case (see eq 22), is not restricted to be between 0 and 1. In most cases, the value of ζ_m is close to unity, which indicates that the perturbative expansion behaves nicely.

III.C. Oscillator Strengths. Oscillator strengths, i.e., transition dipole moments from the ground to the corresponding excited state, are key quantities that are linked to experimental intensities and are usually used to probe the quality of excited-state calculations.[164−167]

For the spin-conserved transitions, the *x* component of the transition dipole moment is

$$\mu^{sc}_{x,m} = \sum_{ia\sigma} (i_\sigma | x | a_\sigma)(\mathbf{X}^{sc}_m + \mathbf{Y}^{sc}_m)_{i_\sigma a_\sigma} \quad (39)$$

where

$$(p_\sigma | x | q_{\sigma'}) = \int \phi_{p_\sigma}(\mathbf{r}) x \phi_{q_{\sigma'}}(\mathbf{r}) \, d\mathbf{r} \quad (40)$$

are one-electron integrals in the orbital basis. The total oscillator strength in the so-called length gauge[167] is given by

$$f^{sc}_m = \frac{2}{3} \Omega^{sc}_m [(\mu^{sc}_{x,m})^2 + (\mu^{sc}_{x,m})^2 + (\mu^{sc}_{x,m})^2] \quad (41)$$

For spin-flip transitions, we have $f^{sf}_m = 0$ as the transition matrix elements $(i_\sigma | x | a_{\bar{\sigma}})$ vanish via integration over the spin coordinate.

III.D. Spin Contamination. One of the key issues of linear response formalism based on unrestricted references is spin contamination or the artificial mixing with configurations of different spin multiplicities. As nicely explained in ref 12, there are two sources of spin contamination: (i) spin contamination of the reference configuration for which, for example, $\langle \hat{S}^2 \rangle > 2$ for high-spin triplets and (ii) spin contamination of the excited states due to spin incompleteness of the CI expansion. The latter issue is an important source of spin contamination in the present context as BSE is limited to single excitations with respect to the reference configuration. Specific schemes have been developed to palliate these shortcomings, and we refer the interested reader to ref 12 for a detailed discussion on this matter.

In order to monitor closely how contaminated are these states, we compute

$$\langle \hat{S}^2 \rangle_m = \langle \hat{S}^2 \rangle_0 + \Delta \langle \hat{S}^2 \rangle_m \quad (42)$$

where

$$\langle \hat{S}^2 \rangle_0 = \frac{n_\uparrow - n_\downarrow}{2} \left(\frac{n_\uparrow - n_\downarrow}{2} + 1 \right) + n_\downarrow - \sum_p (p_\uparrow | p_\downarrow)^2 \quad (43)$$

is the expectation value of $\hat{S}^2$ for the reference configuration, the first term corresponding to the exact value of $\langle \hat{S}^2 \rangle$, and

$$(p_\sigma | q_{\sigma'}) = \int \phi_{p_\sigma}(\mathbf{r}) \phi_{q_{\sigma'}}(\mathbf{r}) \, d\mathbf{r} \quad (44)$$

are overlap integrals between spin-σ and spin-σ' orbitals.

Table 1. Excitation Energies (in eV) with Respect to the $^1S(1s^2\,2s^2)$ Singlet Ground State of Be Obtained at Various Methods with the 6-31G Basis Set[a]

method	excitation energies (eV)				
	$^1S(1s^2\,2s^2)$	$^3P(1s^2\,2s^1\,2p^1)$	$^1P(1s^2\,2s^1\,2p^1)$	$^3P(1s^2\,2p^2)$	$^1D(1s^2\,2p^2)$
SF-TD-BLYP[b]	(0.002)	3.210(1.000)	3.210(1.000)	6.691(1.000)	7.598(0.013)
SF-TD-B3LYP[b]	(0.001)	3.332(1.839)	4.275(0.164)	6.864(1.000)	7.762(0.006)
SF-TD-BH&HLYP[b]	(0.000)	2.874(1.981)	4.922(0.023)	7.112(1.000)	8.188(0.002)
SF-TD-CAM-B3LYP	(0.001)	3.186(1.960)	4.554(0.043)	7.020(1.000)	7.933(0.008)
SF-TD-ωB97X-D	(0.006)	3.337(1.867)	4.717(0.147)	7.076(1.000)	8.247(0.040)
SF-TD-LC-ωPBE08	(0.014)	3.434(1.720)	5.904(0.287)	7.088(1.000)	9.471(0.073)
SF-CIS[c]	(0.002)	2.111(2.000)	6.036(0.014)	7.480(1.000)	8.945(0.006)
SF-BSE@G_0W_0	(0.004)	2.399(1.999)	6.191(0.023)	7.792(1.000)	9.373(0.013)
SF-BSE@evGW	(0.004)	2.407(1.999)	6.199(0.023)	7.788(1.000)	9.388(0.013)
SF-BSE@qsGW	(0.057)	2.376(1.963)	6.241(0.048)	7.668(1.000)	9.417(0.004)
SF-dBSE@G_0W_0		2.363	6.263	7.824	9.424
SF-dBSE@evGW		2.369	6.273	7.820	9.441
SF-dBSE@qsGW		2.335	6.317	7.689	9.470
SF-ADC(2)-s		2.433	6.255	7.745	9.047
SF-ADC(2)-x		2.866	6.581	7.664	8.612
SF-ADC(3)		2.863	6.579	7.658	8.618
FCI[c]	(0.000)	2.862(2.000)	6.577(0.000)	7.669(2.000)	8.624(0.000)

[a]All the spin-flip calculations have been performed with an unrestricted reference. The $\langle \hat{S}^2 \rangle$ value associated with each state is reported in parentheses (when available). [b]Excitation energies taken from ref 12. [c]Excitation energies taken from ref 80.
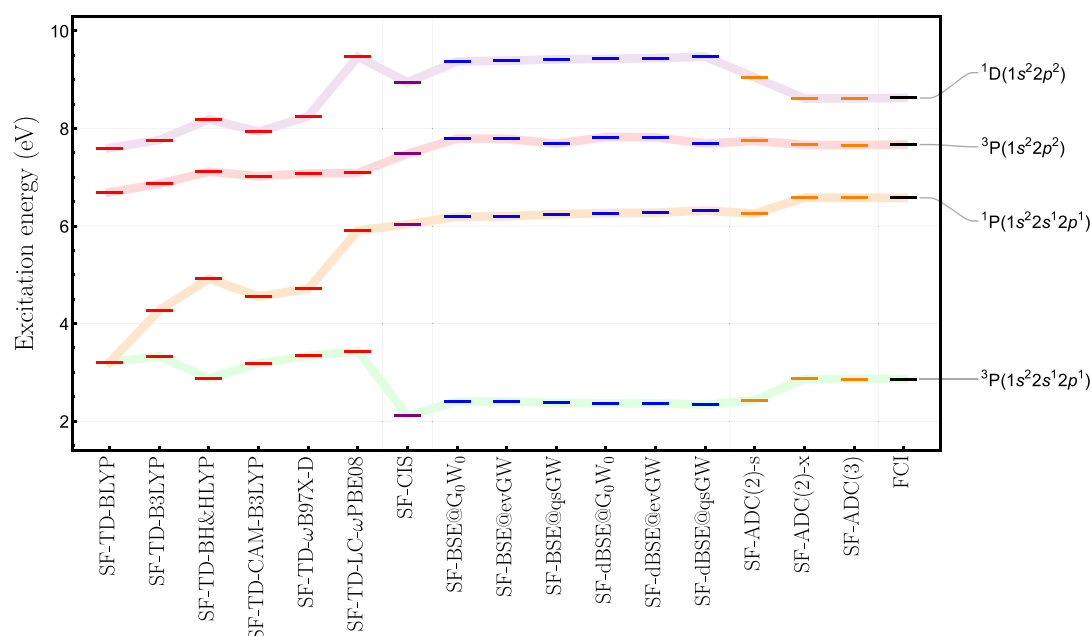

Figure 1. Excitation energies (in eV) with respect to the $^1S(1s^2\,2s^2)$ singlet ground state of Be obtained with the 6-31G basis at various levels of theory: SF-TD-DFT (red), SF-CIS (purple), SF-BSE (blue), SF-ADC (orange), and FCI (black). All the spin-flip calculations have been performed with an unrestricted reference.

For a given single excitation m, the explicit expressions of $\Delta \langle \hat{S}^2 \rangle_m^{sc}$ and $\Delta \langle \hat{S}^2 \rangle_m^{sf}$ can be found in the Appendix of ref 97 for spin-conserved and spin-flip excitations, and they are functions of the vectors $\mathbf{X}_m$ and $\mathbf{Y}_m$ as well as the orbital overlaps defined in eq 44.

IV. COMPUTATIONAL DETAILS

All the systems under investigation here have a closed-shell singlet ground state, and we consider the lowest triplet state as reference for the spin-flip calculations adopting the unrestricted formalism throughout this work. The G_0W_0 calculations performed to obtain the screened Coulomb potential and the

quasiparticle energies required to compute the BSE neutral excitations are performed using an unrestricted Hartree−Fock (UHF) starting point, and the G_0W_0 quasiparticle energies are obtained by linearizing the frequency-dependent quasiparticle equation (see eq 21. Note that the entire set of orbitals and energies is corrected. Further details about our implementation of G_0W_0 can be found in refs 44, 69, 147, 168, and 169.

Here, we do not investigate how the starting orbitals affect the BSE@G_0W_0 excitation energies. This is left for future work. However, it is worth mentioning that, for the present (small) molecular systems, Hartree−Fock is usually a good starting point,[44,69,170] although improvements could certainly be
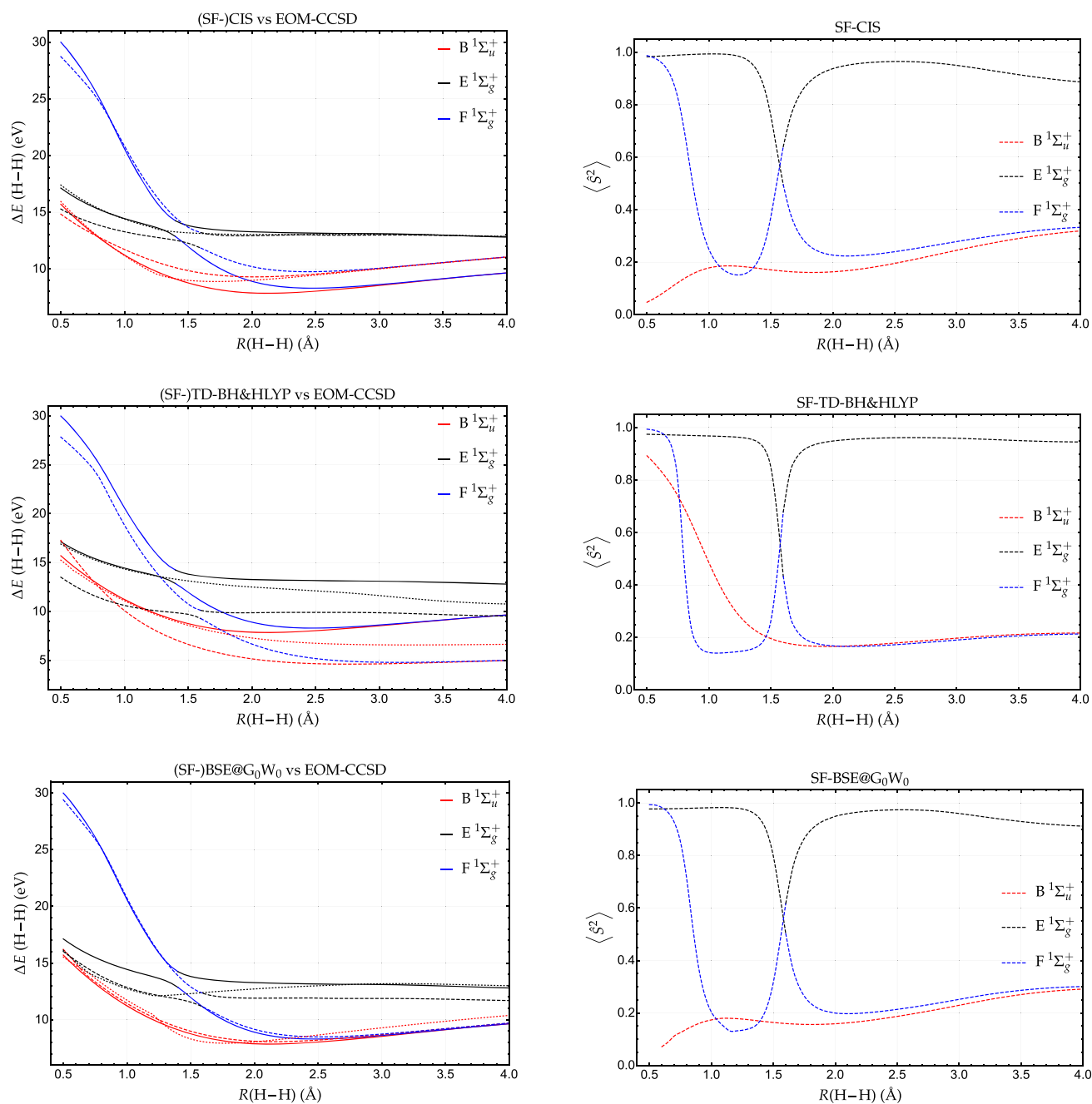
Figure 2. Excitation energies with respect to the X $^1\Sigma_g^+$ ground state (left) and expectation value of the spin operator $\langle \hat{S}^2 \rangle$ (right) of the B $^1\Sigma_u^+$ (red), E $^1\Sigma_g^+$ (black), and F $^1\Sigma_g^+$ (blue) states of H$_2$ obtained with the cc-pVQZ basis at the (SF-)CIS (top), (SF-)TD-BH&HLYP (middle), and (SF-)BSE (bottom) levels of theory. The reference EOM-CCSD excitation energies are represented as solid lines, while the results obtained with and without spin-flip are represented as dashed and dotted lines, respectively. All the spin-conserved and spin-flip calculations have been performed with an unrestricted reference. The raw data are reported in the Supporting Information.

obtained with starting orbitals and energies computed with, for example, optimally tuned range-separated hybrid (RSH) functionals.[171−174] Besides this, G_0W_0@UHF and evGW@UHF yield similar quasiparticle energies, while G_0W_0 allows us to avoid rather laborious iterations as well as the significant additional computational effort of evGW.[44,69,169] In the following, all linear response calculations are performed within the TDA to ensure consistency between the spin-conserved and spin-flip results. Finally, the infinitesimal η is set to 100 meV for all calculations.

All the static and dynamic BSE calculations (labeled in the following as SF-BSE and SF-dBSE respectively) are performed with the software QuAcK,[175] developed in our group and freely available on github. The standard and extended spin-flip ADC(2) calculations [SF-ADC(2)-s and SF-ADC(2)-x, respectively] as well as the SF-ADC(3)[110] are performed with Q-CHEM 5.2.1.[176] Spin-flip TD-DFT calculations[107] (also performed with Q-CHEM 5.2.1) considering the BLYP,[177,178] B3LYP,[177−179] and BH&HLYP[178,180] functionals which contain 0%, 20%, and 50% of exact exchange are labeled as SF-TD-BLYP, SF-TD-B3LYP, and SF-TD-BH&HLYP, respectively.

Additionally, we have performed spin-flip TD-DFT calculations considering the following RSH functionals: CAM-B3LYP,[181] LC-ωPBE08,[182] and ωB97X-D.[183,184] In the present context, the main difference between these RSHs is their amount of exact exchange at long-range: 75% for CAM-B3LYP and 100% for both LC-ωPBE08 and ωB97X-D. EOM-CCSD excitation energies[185−187] are computed with Gaussian 09.[188] As a consistency check, we systematically perform SF-CIS calculations[80] with both QuAcK and Q-CHEM, and make sure that they yield identical excitation energies. Throughout this work, all spin-flip and spin-conserved calculations are performed with an unrestricted reference.

V. RESULTS

V.A. Beryllium Atom. As a first example, we consider the simple case of the beryllium atom in a small basis (6-31G) which was considered by Krylov in two of her very first papers on spin-flip methods.[80,81] It was also considered in later studies thanks to its pedagogical value.[12,93] Beryllium has a ^1S ground state with $1s^2\, 2s^2$ configuration. The excitation energies corresponding to the first singlet and triplet single excitations $2s \rightarrow 2p$ with P spatial symmetries as well as the first singlet and triplet double excitations $2s^2 \rightarrow 2p^2$ with D and P spatial symmetries (respectively) are reported in Table 1 and depicted in Figure 1.

On the left side of Figure 1, we report SF-TD-DFT excitation energies (red lines) obtained with the BLYP, B3LYP, and BH&HLYP functionals, which correspond to an increase of exact exchange from 0% to 50%. As mentioned in ref 12., the $^3P(1s^2\, 2s^1\, 2p^1)$ and the $^1P(1s^2\, 2s^1\, 2p^1)$ states are degenerate at the SF-TD-BLYP level. Indeed, due to the lack of coupling terms in the spin-flip block of the SD-TD-DFT equations (see Section III.A), their excitation energies are given by the energy difference between the 2s and 2p orbitals and both states are strongly spin contaminated. Including exact exchange, like in SF-TD-B3LYP and SF-TD-BH&HLYP, lifts this degeneracy and improves the description of both states. However, the SF-TD-BH&HLYP excitation energy of the $^1P(1s^2\, 2s^1\, 2p^1)$ state is still off by 1.6 eV as compared to the FCI reference. For the other states, the agreement between SF-TD-BH&HLYP and FCI is significantly improved. Spin-flip TD-DFT calculations performed with CAM-B3LYP and ωB97X-D are only slightly more accurate than their global hybrid counterparts, while SF-TD-LC-ωPBE08 yields more significant improvements although it does not reach the accuracy of SF-(d)BSE.

The center part of Figure 1 shows the SF-(d)BSE results (blue lines) alongside the SF-CIS excitation energies (purple lines). All of these are computed with 100% of exact exchange with the additional inclusion of correlation in the case of SF-BSE and SF-dBSE thanks to the introduction of static and dynamical screening, respectively. Overall, the SF-CIS and SF-BSE excitation energies are closer to FCI than the SF-TD-DFT ones, except for the lowest triplet state where the SF-TD-BH&HLYP excitation energy is more accurate probably due to error compensation. At the exception of the ^1D state, SF-BSE improves over SF-CIS with a rather small contribution from the additional dynamical effects included in the SF-dBSE scheme. Note that the exact exchange seems to spin purified the $^3P(1s^2\, 2s^1\, 2p^1)$ state while the singlet states at the SF-BSE level are slightly more spin contaminated than their SF-CIS counterparts.

Table 1 and Figure 1 also gathers results obtained at the partially self-consistent SF-(d)BSE@evGW and fully self-consistent SF-(d)BSE@qsGW levels. The SF-(d)BSE excitation energies are quite stable with respect to the underlying GW

scheme, which nicely illustrates that UHF eigenstates are actually an excellent starting point in this particular case.

The right side of Figure 1 illustrates the performance of the SF-ADC methods. Interestingly, SF-BSE and SF-ADC(2)-s have rather similar accuracies, except again for the ^1D state where SF-ADC(2)-s has clearly the edge over SF-BSE. Finally, both SF-ADC(2)-x and SF-ADC(3) yield excitation energies very close to FCI for this simple system with significant improvements for the lowest ^3P state and the ^1D doubly excited state. Although the (d)BSE and ADC(2)-s have obvious theoretical similarities, we would like to mention that they are not strictly identical as ADC(2) includes key second-order exchange contributions that are not included at the GW level even in the case of more elaborate schemes like evGW and qsGW.

V.B. Hydrogen Molecule. Our second example deals with the dissociation of the H_2 molecule, which is a prototypical system for testing new electronic structure methods and, specifically, their accuracy in the presence of strong correlation (see, for example, refs 189−192 and references therein). The X $^1\Sigma_g^+$ ground state of H_2 has an electronic configuration $(1\sigma_g)^2$ configuration. The variation of the excitation energies associated with the three lowest singlet excited states with respect to the elongation of the H−H bond are of particular interest here. The lowest singly excited state B $^1\Sigma_u^+$ has a $(1\sigma_g)\,(1\sigma_u)$ configuration, while the singly excited state E $^1\Sigma_g^+$ and the doubly excited state F $^1\Sigma_g^+$ have $(1\sigma_g)\,(2\sigma_g)$ and $(1\sigma_u)^2$ configurations, respectively. Because these latter two excited states interact strongly and form an avoided crossing around $R(H-H) = 1.4$ Å, they are usually labeled as the EF $^1\Sigma_g^+$ state. Note that this avoided crossing is not visible with non-spin-flip methods restricted to single excitations (such as CIS, TD-DFT, and BSE) as these are "blind" to double excitations. Three methods, in their standard and spin-flip versions, are studied here (CIS, TD-BH&HLYP, and BSE) and are compared to the reference EOM-CCSD excitation energies (that is equivalent to FCI in the case of H_2). All these calculations are performed with the cc-pVQZ basis.

The top panel of Figure 2 shows the CIS (dotted lines) and SF-CIS (dashed lines) excitation energies as functions of $R(H-H)$. The EOM-CCSD reference energies are represented by solid lines. We observe that both CIS and SF-CIS poorly describe the B $^1\Sigma_u^+$ state in the dissociation limit with an error greater than 1 eV, while CIS, unlike SF-CIS, is much more accurate around the equilibrium geometry. Similar observations can be made for the E $^1\Sigma_g^+$ state with a good description at the CIS level for all bond lengths. SF-CIS does not model accurately the E $^1\Sigma_g^+$ state before the avoided crossing, but the agreement between SF-CIS and EOM-CCSD is much satisfactory for bond length greater than 1.6 Å. Oppositely, SF-CIS describes better the F $^1\Sigma_g^+$ state before the avoided crossing than after, while this state is completely absent at the CIS level. Indeed, as mentioned earlier, CIS is unable to locate any avoided crossing as it cannot access double excitations. At the SF-CIS level, the avoided crossing between the E and F states is qualitatively reproduced and placed at a slightly larger bond length $[R(H-H) \approx 1.5$ Å$]$ than at the EOM-CCSD level.

In the central panel of Figure 2, we report the (SF-)TD-BH&HLYP results. SF-TD-BH&HLYP shows, at best, qualitative agreement with EOM-CCSD, while the TD-BH&HLYP excitation energies of the B and E states are only trustworthy around equilibrium but inaccurate at dissociation. Note that H_2

is a rather challenging system for (SF-)TD-DFT from a general point of view.[191,193−195] Similar graphs for (SF-)TD-BLYP and (SF-)TD-B3LYP are reported in the Supporting Information from which one can draw similar conclusions. Notably, one can see that the E $^1\Sigma_g^+$ and F $^1\Sigma_g^+$ states crossed without interacting at the SF-TD-BLYP level due to the lack of Hartree−Fock exchange. In the Supporting Information, we also report the potential energy curves of H_2 obtained with three RSHs (CAM-B3LYP, ωB97X-D, and LC-ωPBE08), which only brought a modest improvement and rather sharp avoided crossings as compared to EOM-CCSD.

In the bottom panel of Figure 2, (SF-)BSE excitation energies for the same three singlet states are represented. SF-BSE provides surprisingly accurate excitation energies for the B $^1\Sigma_u^+$ state with errors between 0.05 and 0.3 eV, outperforming in the process the standard BSE formalism. However, SF-BSE does not describe well the E $^1\Sigma_g^+$ state with the error ranging from 0.5 to 1.6 eV. Similar performances are observed at the BSE level around equilibrium with a clear improvement in the dissociation limit. Remarkably, SF-BSE shows a good agreement with EOM-CCSD for the F $^1\Sigma_g^+$ doubly excited state, resulting in an avoided crossing around R(H−H) = 1.6 Å. A similar graph comparing (SF-)dBSE and EOM-CCSD excitation energies can be found in the Supporting Information where it is shown that dynamical effects do not affect the present conclusions. One would also notice a little "kink" in the potential energy curves of the B $^1\Sigma_u^+$ and E $^1\Sigma_g^+$ states around R(H−H) = 1.2 Å computed at the (d)BSE@G_0W_0 level. This unfortunate feature is due to the appearance of the symmetry-broken UHF solution and the lack of self-consistency in G_0W_0. Indeed, R = 1.2 Å corresponds to the location of the well-known Coulson-Fischer point.[196] Note that, as mentioned earlier, all the calculations are performed with a UHF reference even the ones based on a closed-shell singlet reference. If one relies solely on the restricted HF solution, this kink disappears and one obtains smooth potential energy curves (see Supporting Information).

The right side of Figure 2 shows the amount of spin contamination as a function of the bond length for SF-CIS (top), SF-TD-BH&HLYP (center), and SF-BSE (bottom). Overall, one can see that $\langle \hat{S}^2 \rangle$ behaves similarly for SF-CIS and SF-BSE with a small spin contamination of the B $^1\Sigma_u^+$ at short bond length. In contrast, the B state is much more spin contaminated at the SF-TD-BH&HLYP level. For all spin-flip methods, the E state is strongly spin contaminated as expected, while the $\langle \hat{S}^2 \rangle$ values associated with the F state only deviate significantly from zero for short bond length and around the avoided crossing where it strongly couples with the spin-contaminated E state.

V.C. Cyclobutadiene. Cyclobutadiene (CBD) is an interesting example as the electronic character of its ground state can be tuned via geometrical deformation.[12,101,102,110,197−201] In the D_{2h} rectangular geometry of the A_g singlet ground state, the highest occupied molecular orbital (HOMO) and lowest unoccupied molecular orbital (LUMO) are nondegenerate, and the singlet ground state can be safely labeled as single-reference with well-defined doubly occupied orbitals. However, in the D_{4h} square-planar geometry of the A_{2g} triplet state, the HOMO and LUMO are strictly degenerate, and the electronic ground state, which is still of singlet nature with B_{1g} spatial symmetry (hence violating Hund's rule), is strongly multireference with singly occupied orbitals (i.e., singlet open-shell state). In this case, single-reference methods notoriously fail. Nonetheless, the lowest triplet state of symmetry $^3A_{2g}$ remains of single-reference character and is then a perfect

starting point for spin-flip calculations. The D_{2h} and D_{4h} optimized geometries of the ^1A_g and $^3A_{2g}$ states of CBD have been extracted from ref 102 and have been obtained at the CCSD(T)/cc-pVTZ level. For comparison purposes, EOM-SF-CCSD and SF-ADC excitation energies have been extracted from ref 102 and ref 110, respectively. All of them have been obtained with a UHF reference like the SF-BSE calculations performed here.

Tables 2 and 3 report excitation energies (with respect to the singlet ground state) obtained at the D_{2h} and D_{4h} geometries,

Table 2. Vertical Excitation Energies (with Respect to the Singlet X ^1A_g Ground State) of the 1 $^3B_{1g}$, 1 $^1B_{1g}$, and 2 ^1A_g States of CBD at the D_{2h} Rectangular Equilibrium Geometry of the X ^1A_g Ground State[a]

	excitation energies (eV)		
method	1 $^3B_{1g}$	1 $^1B_{1g}$	2 ^1A_g
SF-TD-B3LYP[b]	1.750	2.260	4.094
SF-TD-BH&HLYP[b]	1.583	2.813	4.528
SF-TD-CAM-B3LYP	1.790	2.379	4.238
SF-TD-ωB97X-D	1.771	2.366	4.212
SF-TD-LC-ωPBE08	1.941	2.464	4.428
SF-CIS[c]	1.521	3.836	5.499
EOM-SF-CCSD[d]	1.654	3.416	4.360
EOM-SF-CCSD(fT)[d]	1.516	3.260	4.205
EOM-SF-CCSD(dT)[d]	1.475	3.215	4.176
SF-ADC(2)-s[e]	1.573	3.208	4.247
SF-ADC(2)-x[e]	1.576	3.141	3.796
SF-ADC(3)[c]	1.456	3.285	4.334
SF-BSE@G_0W_0[b]	1.438	2.704	4.540
SF-dBSE@G_0W_0[b]	1.403	2.883	4.621

[a]All the spin-flip calculations have been performed with an unrestricted reference and the cc-pVTZ basis set. [b]This work. [c]Values from ref 12. [d]Values from ref 102. [e]Values from ref 110.

Table 3. Vertical Excitation Energies (with Respect to the Singlet X $^1B_{1g}$ Ground State) of the 1 $^3A_{2g}$, 2 $^1A_{1g}$, and 1 $^1B_{2g}$ States of CBD at the D_{4h} Square-Planar Equilibrium Geometry of the 1 $^3A_{2g}$ State[a]

	excitation energies (eV)		
method	1 $^3A_{2g}$	2 $^1A_{1g}$	1 $^1B_{2g}$
SF-TD-B3LYP[b]	−0.020	0.547	0.486
SF-TD-BH&HLYP[b]	0.048	1.465	1.282
SF-TD-CAM-B3LYP	0.012	0.677	0.595
SF-TD-ωB97X-D	0.005	0.673	0.592
SF-TD-LC-ωPBE08	0.062	0.663	0.570
SF-CIS[c]	0.317	3.125	2.650
EOM-SF-CCSD[d]	0.369	1.824	2.143
EOM-SF-CCSD(fT)[d]	0.163	1.530	1.921
EOM-SF-CCSD(dT)[d]	0.098	1.456	1.853
SF-ADC(2)-s[e]	0.266	1.664	1.910
SF-ADC(2)-x[e]	0.217	1.123	1.799
SF-ADC(3)[e]	0.083	1.621	1.930
SF-BSE@G_0W_0[b]	−0.092	1.189	1.480
SF-dBSE@G_0W_0[b]	0.012	1.507	1.841

[a]All the spin-flip calculations have been performed with an unrestricted reference and the cc-pVTZ basis set. [b]This work. [c]Values from ref 12. [d]Values from ref 102. [e]Values from ref 110.

respectively, for several methods using the spin-flip *ansatz*. All these results are represented in Figure 3. For each geometry,
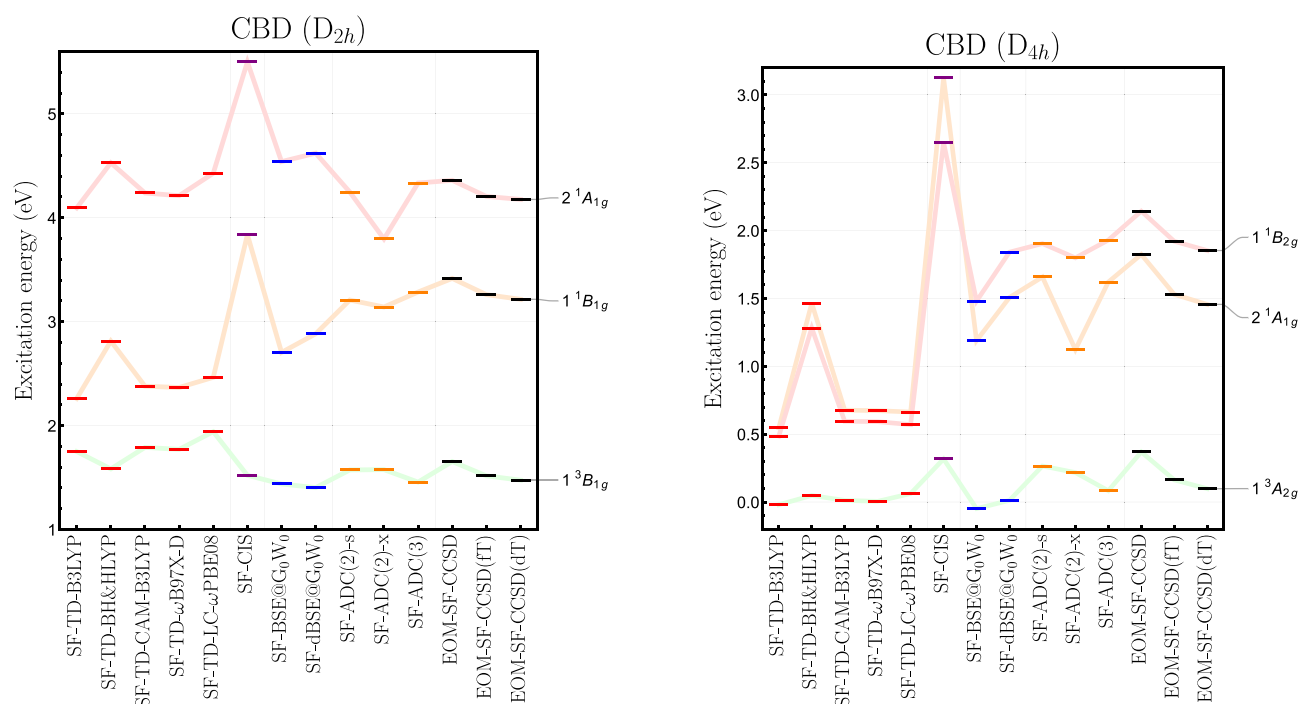
Figure 3. Vertical excitation energies of CBD at various levels of theory: SF-TD-DFT (red), SF-CIS (purple), SF-BSE (blue), SF-ADC (orange), and EOM-SF-CCSD (black). Left: $1\ ^3B_{1g}$, $1\ ^1B_{1g}$, and $2\ ^1A_{1g}$ states at the D_{2h} rectangular equilibrium geometry of the X ^1A_g ground state (see Table 2 for the raw data). Right: $1\ ^3A_{2g}$, $2\ ^1A_{1g}$, and $1\ ^1B_{2g}$ states at the D_{4h} square-planar equilibrium geometry of the $1\ ^3A_{2g}$ state (see Table 3 for the raw data). All the spin-flip calculations have been performed with an unrestricted reference and the cc-pVTZ basis set.

three excited states are under investigation: (i) the $1\ ^3B_{1g}$, $1\ ^1B_{1g}$, and $2\ ^1A_g$ states of the D_{2h} geometry; (ii) the $1\ ^3A_{2g}$, $2\ ^1A_{1g}$, and $1\ ^1B_{2g}$ states of the D_{4h} geometry. It is important to mention that the $2\ ^1A_{1g}$ state of the rectangular geometry has a significant double excitation character,[57] and it is then barely described by second-order methods [such as CIS(D),[202,203] ADC(2),[204,205] CC2,[206] or EOM-CCSD[185−187]] and remains a real challenge for third-order methods [as, for example, ADC(3),[164,205,207] CC3,[74] or EOM-CCSDT[76−79]].

Comparing the present SF-BSE@G_0W_0 results for the rectangular geometry (see Table 2) to the most accurate ADC level, i.e., SF-ADC(3), we have a difference in excitation energy of 0.017 eV for the $1\ ^3B_{1g}$ state. This difference grows to 0.572 eV for the $1\ ^1B_{1g}$ state and then shrinks to 0.212 eV for the $2\ ^1A_g$ state. Overall, adding dynamical corrections via the SF-dBSE@G_0W_0 scheme does not improve the accuracy of the excitation energies [as compared to SF-ADC(3)] with errors of 0.052, 0.393, and 0.293 eV for the $1\ ^3B_{1g}$, $1\ ^1B_{1g}$, and $2\ ^1A_g$ states, respectively.

Now, looking at Table 3 which gathers the results for the square-planar geometry, we see that, at the SF-BSE@G_0W_0 level, the first two states are wrongly ordered with the triplet $1\ ^3B_{1g}$ state lower than the singlet $1\ ^1A_g$ state. (The same observation can be made at the SF-TD-B3LYP level.) This is certainly due to the poor Hartree−Fock reference which lacks opposite-spin correlation and this issue could be potentially alleviated by using a better starting point for the GW calculation, as discussed in Section IV. Nonetheless, it is pleasing to see that adding the dynamical correction in SF-dBSE@G_0W_0 not only improves the agreement with SF-ADC(3) but also retrieves the right state ordering. Then, CBD stands as an excellent example for which dynamical corrections are necessary to get the right chemistry at the SF-BSE level. Another interesting feature is the wrong ordering of the $2\ ^1A_{1g}$ and $1\ ^1B_{2g}$ states at the SF-B3LYP, SF-

BH&HLYP, and SF-CIS levels which give the former higher in energy than the latter. This issue does not appear at the SF-BSE, SF-ADC, and SF-EOM-SF-CCSD levels. Here again, one does not observe a clear improvement by considering RSHs instead of global hybrids (BH&HLYP seems to perform particularly well in the case of CBD), although it is worth mentioning that RSH-based SF-TD-DFT calculations yield accurate excitation for the double excitation $1\ ^1A_g \rightarrow 2\ ^1A_g$ in the D_{2h} geometry.

VI. CONCLUSION

In this article, we have presented the extension of the BSE approach of many-body perturbation theory to the spin-flip formalism in order to access double excitations in realistic molecular systems. The present spin-flip calculations rely on a spin-unrestricted version of the GW approximation and the BSE formalism with, on top of this, a dynamical correction to the static BSE optical excitations via an unrestricted generalization of our recently developed renormalized perturbative treatment. Taking the beryllium atom, the dissociation of the hydrogen molecule, and cyclobutadiene in two different geometries as examples, we have shown that the spin-flip BSE formalism can accurately model double excitations and seems to surpass systematically its spin-flip TD-DFT parent. Further improvements could be obtained thanks to a better choice of the starting orbitals and their energies, and we hope to investigate this in a forthcoming paper. Techniques to alleviate the spin contamination in spin-flip BSE will also be explored in the near future. We hope that these new encouraging results will stimulate new developments around the BSE formalism to further establish it as a valuable *ab inito* alternative to TD-DFT for the study of molecular excited states.

■ ASSOCIATED CONTENT

ⓢ Supporting Information

The Supporting Information is available free of charge at https://pubs.acs.org/doi/10.1021/acs.jctc.1c00074.

Additional graphs comparing (SF-)TD-DFT and (SF-)dBSE with EOM-CCSD for the H_2 molecule and raw data associated with Figure 2 (PDF)

■ AUTHOR INFORMATION

Corresponding Author

Pierre-François Loos − *Laboratoire de Chimie et Physique Quantiques (UMR 5626), Université de Toulouse, CNRS, UPS, 31062 Toulouse, France;* ⓞ orcid.org/0000-0003-0598-7425; Email: loos@irsamc.ups-tlse.fr

Author

Enzo Monino − *Laboratoire de Chimie et Physique Quantiques (UMR 5626), Université de Toulouse, CNRS, UPS, 31062 Toulouse, France*

Complete contact information is available at:
https://pubs.acs.org/10.1021/acs.jctc.1c00074

Notes

The authors declare no competing financial interest.

■ ACKNOWLEDGMENTS

■ REFERENCES

(1) Roos, B. O.; Andersson, K.; Fulscher, M. P.; Malmqvist, P.-A.; Serrano-Andrés, L.; Prigogine, I.; Rice, S. A. Multiconfigurational Perturbation Theory: Applications In Electronic Spectroscopy. *Adv. Chem. Phys.* **1996**, *93*, 219−331.

(2) Piecuch, P.; Kowalski, K.; Pimienta, I. S. O.; Mcguire, M. J. Recent advances in electronic structure theory: Method of moments of coupled-cluster equations and renormalized coupled-cluster approaches. *Int. Rev. Phys. Chem.* **2002**, *21*, 527−655.

(3) Dreuw, A.; Head-Gordon, M. Single-Reference Ab Initio Methods for the Calculation of Excited States of Large Molecules. *Chem. Rev.* **2005**, *105*, 4009−4037.

(4) Krylov, A. I. Spin-Flip Equation-of-Motion Coupled-Cluster Electronic Structure Method for a Description of Excited States, Bond Breaking, Diradicals, and Triradicals. *Acc. Chem. Res.* **2006**, *39*, 83−91.

(5) Sneskov, K.; Christiansen, O. Excited State Coupled Cluster Methods. *WIREs Comput. Mol. Sci.* **2012**, *2*, 566−584.

(6) González, L.; Escudero, D.; Serrano-Andrès, L. Progress and Challenges in the Calculation of Electronic Excited States. *ChemPhysChem* **2012**, *13*, 28−51.

(7) Laurent, A. D.; Jacquemin, D. TD-DFT Benchmarks: A Review. *Int. J. Quantum Chem.* **2013**, *113*, 2019−2039.

(8) Adamo, C.; Jacquemin, D. The Calculations of Excited-State Properties with Time-Dependent Density Functional Theory. *Chem. Soc. Rev.* **2013**, *42*, 845−856.

(9) Ghosh, S.; Verma, P.; Cramer, C. J.; Gagliardi, L.; Truhlar, D. G. Combining Wave Function Methods with Density Functional Theory for Excited States. *Chem. Rev.* **2018**, *118*, 7249−7292.

(10) Blase, X.; Duchemin, I.; Jacquemin, D.; Loos, P.-F. The Bethe−Salpeter Equation Formalism: From Physics to Chemistry. *J. Phys. Chem. Lett.* **2020**, *11*, 7371−7382.

(11) Loos, P.-F.; Scemama, A.; Jacquemin, D. The Quest for Highly Accurate Excitation Energies: A Computational Perspective. *J. Phys. Chem. Lett.* **2020**, *11*, 2374−2383.

(12) Casanova, D.; Krylov, A. I. Spin-Flip Methods in Quantum Chemistry. *Phys. Chem. Chem. Phys.* **2020**, *22*, 4326.

(13) Salpeter, E. E.; Bethe, H. A. A Relativistic Equation for Bound-State Problems. *Phys. Rev.* **1951**, *84*, 1232.

(14) Sham, L. J.; Rice, T. M. Many-Particle Derivation of the Effective-Mass Equation for the Wannier Exciton. *Phys. Rev.* **1966**, *144*, 708−714.

(15) Strinati, G. Effects of Dynamical Screening on Resonances at Inner-Shell Thresholds in Semiconductors. *Phys. Rev. B: Condens. Matter Mater. Phys.* **1984**, *29*, 5718.

(16) Delerue, C.; Lannoo, M.; Allan, G. Excitonic and Quasiparticle Gaps in Si Nanocrystals. *Phys. Rev. Lett.* **2000**, *84*, 2457−2460.

(17) Strinati, G. Application of the Green's Functions Method to the Study of the Optical Properties of Semiconductors. *Riv. Nuovo Cimento* **1988**, *11*, 1−86.

(18) Albrecht, S.; Reining, L.; Del Sole, R.; Onida, G. Ab Initio Calculation of Excitonic Effects in the Optical Spectra of Semiconductors. *Phys. Rev. Lett.* **1998**, *80*, 4510−4513.

(19) Rohlfing, M.; Louie, S. G. Electron-Hole Excitations in Semiconductors and Insulators. *Phys. Rev. Lett.* **1998**, *81*, 2312−2315.

(20) Benedict, L. X.; Shirley, E. L.; Bohn, R. B. Optical Absorption of Insulators and the Electron-Hole Interaction: An Ab Initio Calculation. *Phys. Rev. Lett.* **1998**, *80*, 4514−4517.

(21) van der Horst, J.-W.; Bobbert, P. A.; Michels, M. A. J.; Brocks, G.; Kelly, P. J. Ab Initio Calculation of the Electronic and Optical Excitations in Polythiophene: Effects of Intra- and Interchain Screening. *Phys. Rev. Lett.* **1999**, *83*, 4413−4416.

(22) Blase, X.; Duchemin, I.; Jacquemin, D. The Bethe−Salpeter equation in chemistry: relations with TD-DFT, applications and challenges. *Chem. Soc. Rev.* **2018**, *47*, 1022−1043.

(23) Onida, G.; Reining, L.; Rubio, A. Electronic Excitations: Density-Functional Versus Many-Body Green's Function Approaches. *Rev. Mod. Phys.* **2002**, *74*, 601−659.

(24) Martin, R. M.; Reining, L.; Ceperley, D. M. *Interacting Electrons: Theory and Computational Approaches*; Cambridge University Press: 2016.

(25) Hedin, L. New Method for Calculating the One-Particle Green's Function with Application to the Electron-Gas Problem. *Phys. Rev.* **1965**, *139*, A796.

(26) Golze, D.; Dvorak, M.; Rinke, P. The GW Compendium: A Practical Guide to Theoretical Photoemission Spectroscopy. *Front. Chem.* **2019**, *7*, 377.

(27) Rohlfing, M.; Louie, S. G. Optical Excitations in Conjugated Polymers. *Phys. Rev. Lett.* **1999**, *82*, 1959−1962.

(28) van der Horst, J.-W.; Bobbert, P. A.; Michels, M. A. J.; Brocks, G.; Kelly, P. J. Ab Initio Calculation of the Electronic and Optical Excitations in Polythiophene: Effects of Intra- and Interchain Screening. *Phys. Rev. Lett.* **1999**, *83*, 4413−4416.

(29) Puschnig, P.; Ambrosch-Draxl, C. Suppression of Electron-Hole Correlations in 3D Polymer Materials. *Phys. Rev. Lett.* **2002**, *89*, 056405.

(30) Tiago, M. L.; Northrup, J. E.; Louie, S. G. Ab Initio Calculation of the Electronic and Optical Properties of Solid Pentacene. *Phys. Rev. B: Condens. Matter Mater. Phys.* **2003**, *67*, 115212.

(31) Boulanger, P.; Jacquemin, D.; Duchemin, I.; Blase, X. Fast and Accurate Electronic Excitations in Cyanines with the Many-Body Bethe−Salpeter Approach. *J. Chem. Theory Comput.* **2014**, *10*, 1212−1218.

(32) Jacquemin, D.; Duchemin, I.; Blase, X. Benchmarking the Bethe−Salpeter Formalism on a Standard Organic Molecular Set. *J. Chem. Theory Comput.* **2015**, *11*, 3290−3304.

(33) Bruneval, F.; Hamed, S. M.; Neaton, J. B. A systematic benchmark of the ab initio Bethe−Salpeter equation approach for low-lying optical excitations of small organic molecules. *J. Chem. Phys.* **2015**, *142*, 244101.

(34) Jacquemin, D.; Duchemin, I.; Blase, X. 0−0 Energies Using Hybrid Schemes: Benchmarks of TD-DFT, CIS(D), ADC(2), CC2,

and BSE/GW formalisms for 80 Real-Life Compounds. *J. Chem. Theory Comput.* **2015**, *11*, 5340–5359.

(35) Hirose, D.; Noguchi, Y.; Sugino, O. All-Electron GW+Bethe–Salpeter Calculations on Small Molecules. *Phys. Rev. B: Condens. Matter Mater. Phys.* **2015**, *91*, 205111.

(36) Jacquemin, D.; Duchemin, I.; Blase, X. Is the Bethe–Salpeter Formalism Accurate for Excitation Energies? Comparisons with TD-DFT, CASPT2, and EOM-CCSD. *J. Phys. Chem. Lett.* **2017**, *8*, 1524–1529.

(37) Jacquemin, D.; Duchemin, I.; Blondel, A.; Blase, X. Benchmark of Bethe–Salpeter for Triplet Excited-States. *J. Chem. Theory Comput.* **2017**, *13*, 767–783.

(38) Rangel, T.; Hamed, S. M.; Bruneval, F.; Neaton, J. B. An Assessment of Low-Lying Excitation Energies and Triplet Instabilities of Organic Molecules with an Ab Initio Bethe–Salpeter Equation Approach and the Tamm-Dancoff Approximation. *J. Chem. Phys.* **2017**, *146*, 194108.

(39) Krause, K.; Klopper, W. Implementation of the Bethe–Salpeter equation in the TURBOMOLE program. *J. Comput. Chem.* **2017**, *38*, 383–388.

(40) Gui, X.; Holzer, C.; Klopper, W. Accuracy Assessment of GW Starting Points for Calculating Molecular Excitation Energies Using the Bethe–Salpeter Formalism. *J. Chem. Theory Comput.* **2018**, *14*, 2127–2136.

(41) Liu, C.; Kloppenburg, J.; Yao, Y.; Ren, X.; Appel, H.; Kanai, Y.; Blum, V. All-electron ab initio Bethe–Salpeter equation approach to neutral excitations in molecules with numeric atom-centered orbitals. *J. Chem. Phys.* **2020**, *152*, 044105.

(42) Holzer, C.; Klopper, W. Communication: A hybrid Bethe–Salpeter/time-dependent density-functional-theory approach for excitation energies. *J. Chem. Phys.* **2018**, *149*, 101101.

(43) Holzer, C.; Gui, X.; Harding, M. E.; Kresse, G.; Helgaker, T.; Klopper, W. Bethe–Salpeter Correlation Energies of Atoms and Molecules. *J. Chem. Phys.* **2018**, *149*, 144106.

(44) Loos, P.-F.; Scemama, A.; Duchemin, I.; Jacquemin, D.; Blase, X. Pros and Cons of the Bethe–Salpeter Formalism for Ground-State Energies. *J. Phys. Chem. Lett.* **2020**, *11*, 3536–3545.

(45) Bruneval, F.; Rangel, T.; Hamed, S. M.; Shao, M.; Yang, C.; Neaton, J. B. Molgw 1: Many-Body Perturbation Theory Software for Atoms, Molecules, and Clusters. *Comput. Phys. Commun.* **2016**, *208*, 149–161.

(46) Runge, E.; Gross, E. K. U. Density-Functional Theory for Time-Dependent Systems. *Phys. Rev. Lett.* **1984**, *52*, 997–1000.

(47) Casida, M. E.; Chong, D. P. Time-Dependent Density Functional Response Theory for Molecules. *Recent Advances in Density Functional Methods* **1995**, *1*, 155–192.

(48) Petersilka, M.; Gossmann, U. J.; Gross, E. K. U. Excitation Energies From Time-Dependent Density-Functional Theory. *Phys. Rev. Lett.* **1996**, *76*, 1212.

(49) Ullrich, C. *Time-Dependent Density-Functional Theory: Concepts and Applications*; Oxford Graduate Texts, Oxford University Press: New York, 2012.

(50) Maitra, N. T.; Zhang, F.; Cave, R. J.; Burke, K. Double excitations within time-dependent density functional theory linear response. *J. Chem. Phys.* **2004**, *120*, 5932.

(51) Cave, R. J.; Zhang, F.; Maitra, N. T.; Burke, K. A Dressed TDDFT Treatment of the 21Ag States of Butadiene and Hexatriene. *Chem. Phys. Lett.* **2004**, *389*, 39–42.

(52) Saha, B.; Ehara, M.; Nakatsuji, H. Singly and Doubly Excited States of Butadiene, Acrolein, and Glyoxal: Geometries and Electronic Spectra. *J. Chem. Phys.* **2006**, *125*, 014316.

(53) Watson, M. A.; Chan, G. K.-L. Excited States of Butadiene to Chemical Accuracy: Reconciling Theory and Experiment. *J. Chem. Theory Comput.* **2012**, *8*, 4013–4018.

(54) Shu, Y.; Truhlar, D. G. Doubly Excited Character or Static Correlation of the Reference State in the Controversial 2 ^{1}A$_g$ State of Trans -Butadiene? *J. Am. Chem. Soc.* **2017**, *139*, 13770–13778.

(55) Barca, G. M. J.; Gilbert, A. T. B.; Gill, P. M. W. Simple Models for Difficult Electronic Excitations. *J. Chem. Theory Comput.* **2018**, *14*, 1501–1509.

(56) Barca, G. M. J.; Gilbert, A. T. B.; Gill, P. M. W. Excitation Number: Characterizing Multiply Excited States. *J. Chem. Theory Comput.* **2018**, *14*, 9–13.

(57) Loos, P.-F.; Boggio-Pasqua, M.; Scemama, A.; Caffarel, M.; Jacquemin, D. Reference Energies for Double Excitations. *J. Chem. Theory Comput.* **2019**, *15*, 1939–1956.

(58) Casida, M. E. Propagator corrections to adiabatic time-dependent density-functional theory linear response theory. *J. Chem. Phys.* **2005**, *122*, 054111.

(59) Huix-Rotllant, M.; Ipatov, A.; Rubio, A.; Casida, M. E. Assessment of Dressed Time-Dependent Density-Functional Theory for the Low-Lying Valence States of 28 Organic Chromophores. *Chem. Phys.* **2011**, *391*, 120–129.

(60) Loos, P.-F.; Scemama, A.; Boggio-Pasqua, M.; Jacquemin, D. Mountaineering Strategy to Excited States: Highly Accurate Energies and Benchmarks for Exotic Molecules and Radicals. *J. Chem. Theory Comput.* **2020**, *16*, 3720–3736.

(61) Levine, B. G.; Ko, C.; Quenneville, J.; Martinez, T. J. Conical Intersections and Double Excitations in Time-Dependent Density Functional Theory. *Mol. Phys.* **2006**, *104*, 1039–1051.

(62) Tozer, D. J.; Handy, N. C. On the Determination of Excitation Energies Using Density Functional Theory. *Phys. Chem. Chem. Phys.* **2000**, *2*, 2117–2121.

(63) Elliott, P.; Goldson, S.; Canahui, C.; Maitra, N. T. Perspectives on Double-Excitations in TDDFT. *Chem. Phys.* **2011**, *391*, 110–119.

(64) Maitra, N. T.; Marques, M. A.; Maitra, N. T.; Nogueira, F. M.; Gross, E.; Rubio, A. *Lect. Notes Phys.* **2012**, *837*, 167–184.

(65) Maitra, N. T. Fundamental aspects of time-dependent density functional theory. *J. Chem. Phys.* **2016**, *144*, 220901.

(66) Ankudinov, A. L.; Nesvizhskii, A. I.; Rehr, J. J. Dynamic Screening Effects in X-Ray Absorption Spectra. *Phys. Rev. B: Condens. Matter Mater. Phys.* **2003**, *67*, 115120.

(67) Romaniello, P.; Sangalli, D.; Berger, J. A.; Sottile, F.; Molinari, L. G.; Reining, L.; Onida, G. Double excitations in finite systems. *J. Chem. Phys.* **2009**, *130*, 044108.

(68) Sangalli, D.; Romaniello, P.; Onida, G.; Marini, A. Double Excitations in Correlated Systems: A Many-Body Approach. *J. Chem. Phys.* **2011**, *134*, 034115.

(69) Loos, P.-F.; Blase, X. Dynamical correction to the Bethe–Salpeter equation beyond the plasmon-pole approximation. *J. Chem. Phys.* **2020**, *153*, 114120.

(70) Authier, J.; Loos, P.-F. Dynamical kernels for optical excitations. *J. Chem. Phys.* **2020**, *153*, 184105.

(71) Loos, P. F.; Scemama, A.; Blondel, A.; Garniron, Y.; Caffarel, M.; Jacquemin, D. A Mountaineering Strategy to Excited States: Highly-Accurate Reference Energies and Benchmarks. *J. Chem. Theory Comput.* **2018**, *14*, 4360.

(72) Loos, P. F.; Lipparini, F.; Boggio-Pasqua, M.; Scemama, A.; Jacquemin, D. A Mountaineering Strategy to Excited States: Highly-Accurate Energies and Benchmarks for Medium Sized Molecules. *J. Chem. Theory Comput.* **2020**, *16*, 1711–1741.

(73) Véril, M.; Scemama, A.; Caffarel, M.; Lipparini, F.; Boggio-Pasqua, M.; Jacquemin, D.; Loos, P.-F. QUESTDB: a database of highly-accurate excitation energies for the electronic structure community. *WIREs* **2021**, DOI: 10.1002/wcms.1517.

(74) Christiansen, O.; Koch, H.; Jørgensen, P. Response Functions in the CC3 Iterative Triple Excitation Model. *J. Chem. Phys.* **1995**, *103*, 7429–7441.

(75) Koch, H.; Christiansen, O.; Jorgensen, P.; Sanchez de Merás, A. M.; Helgaker, T. The CC3Model: An Iterative Coupled Cluster Approach Including Connected Triples. *J. Chem. Phys.* **1997**, *106*, 1808–1818.

(76) Kucharski, S. A.; Bartlett, R. J. Recursive Intermediate Factorization and Complete Computational Linearization of the Coupled-Cluster Single, Double, Triple, and Quadruple Excitation Equations. *Theor. Chim. Acta* **1991**, *80*, 387–405.

(77) Kállay, M.; Gauss, J. Calculation of Excited-State Properties Using General Coupled-Cluster and Configuration-Interaction Models. *J. Chem. Phys.* **2004**, *121*, 9257−9269.

(78) Hirata, S.; Nooijen, M.; Bartlett, R. J. High-Order Determinantal Equation-of-Motion Coupled-Cluster Calculations for Electronic Excited States. *Chem. Phys. Lett.* **2000**, *326*, 255−262.

(79) Hirata, S. Higher-Order Equation-of-Motion Coupled-Cluster Methods. *J. Chem. Phys.* **2004**, *121*, 51−59.

(80) Krylov, A. I. Size-consistent wave functions for bond-breaking: the equation-of-motion spin-flip model. *Chem. Phys. Lett.* **2001**, *338*, 375−384.

(81) Krylov, A. I. Spin-Flip Configuration Interaction: An Electronic Structure Model That Is Both Variational and Size-Consistent. *Chem. Phys. Lett.* **2001**, *350*, 522−530.

(82) Krylov, A. I.; Sherrill, C. D. Perturbative corrections to the equation-of-motion spin-flip self-consistent field model: Application to bond-breaking and equilibrium properties of diradicals. *J. Chem. Phys.* **2002**, *116*, 3194−3203.

(83) Bethe, H. Zur Theorie der Metalle. *Eur. Phys. J. A* **1931**, *71*, 205−226.

(84) Shibuya, T.-I.; McKoy, V. Higher Random-Phase Approximation as an Approximation to the Equations of Motion. *Phys. Rev. A: At., Mol., Opt. Phys.* **1970**, *2*, 2208−2218.

(85) Krylov, A. I. Equation-of-Motion Coupled-Cluster Methods for Open-Shell and Electronically Excited Species: The Hitchhiker's Guide to Fock Space. *Annu. Rev. Phys. Chem.* **2008**, *59*, 433−462.

(86) Peng, D.; Steinmann, S. N.; van Aggelen, H.; Yang, W. Equivalence of Particle-Particle Random Phase Approximation Correlation Energy and Ladder-Coupled-Cluster Doubles. *J. Chem. Phys.* **2013**, *139*, 104112.

(87) Yang, Y.; van Aggelen, H.; Yang, W. Double, Rydberg and charge transfer excitations from pairing matrix fluctuation and particle-particle random phase approximation. *J. Chem. Phys.* **2013**, *139*, 224105.

(88) Yang, Y.; Peng, D.; Lu, J.; Yang, W. Excitation energies from particle-particle random phase approximation: Davidson algorithm and benchmark studies. *J. Chem. Phys.* **2014**, *141*, 124104.

(89) Peng, D.; Yang, Y.; Zhang, P.; Yang, W. Restricted second random phase approximations and Tamm-Dancoff approximations for electronic excitation energy calculations. *J. Chem. Phys.* **2014**, *141*, 214102.

(90) Zhang, D.; Yang, W. Accurate and efficient calculation of excitation energies with the active-space particle-particle random phase approximation. *J. Chem. Phys.* **2016**, *145*, 144105.

(91) Sutton, C.; Yang, Y.; Zhang, D.; Yang, W. Single, Double Electronic Excitations and Exciton Effective Conjugation Lengths in π-Conjugated Systems. *J. Phys. Chem. Lett.* **2018**, *9*, 4029−4036.

(92) Krylov, A. I. Spin-contamination of coupled-cluster wave functions. *J. Chem. Phys.* **2000**, *113*, 6052−6062.

(93) Sears, J. S.; Sherrill, C. D.; Krylov, A. I. A spin-complete version of the spin-flip approach to bond breaking: What is the impact of obtaining spin eigenfunctions? *J. Chem. Phys.* **2003**, *118*, 9084−9094.

(94) Casanova, D.; Head-Gordon, M. The spin-flip extended single excitation configuration interaction method. *J. Chem. Phys.* **2008**, *129*, 064104.

(95) Huix-Rotllant, M.; Natarajan, B.; Ipatov, A.; Muhavini Wawire, C.; Deutsch, T.; Casida, M. E. Assessment of Noncollinear Spin-Flip Tamm−Dancoff Approximation Time-Dependent Density-Functional Theory for the Photochemical Ring-Opening of Oxirane. *Phys. Chem. Chem. Phys.* **2010**, *12*, 12811.

(96) Li, Z.; Liu, W. Spin-adapted open-shell random phase approximation and time-dependent density functional theory. I. Theory. *J. Chem. Phys.* **2010**, *133*, 064106.

(97) Li, Z.; Liu, W.; Zhang, Y.; Suo, B. Spin-adapted open-shell time-dependent density functional theory. II. Theory and pilot application. *J. Chem. Phys.* **2011**, *134*, 134101.

(98) Li, Z.; Liu, W. Spin-adapted open-shell time-dependent density functional theory. III. An even better and simpler formulation. *J. Chem. Phys.* **2011**, *135*, 194106.

(99) Zhang, X.; Herbert, J. M. Analytic Derivative Couplings in Time-Dependent Density Functional Theory: Quadratic Response Theory versus Pseudo-Wavefunction Approach. *J. Chem. Phys.* **2015**, *142*, 064109.

(100) Lee, S.; Filatov, M.; Lee, S.; Choi, C. H. Eliminating spin-contamination of spin-flip time dependent density functional theory within linear response formalism by the use of zeroth-order mixed-reference (MR) reduced density matrix. *J. Chem. Phys.* **2018**, *149*, 104101.

(101) Levchenko, S. V.; Krylov, A. I. Equation-of-motion spin-flip coupled-cluster model with single and double substitutions: Theory and application to cyclobutadiene. *J. Chem. Phys.* **2004**, *120*, 175−185.

(102) Manohar, P. U.; Krylov, A. I. A noniterative perturbative triples correction for the spin-flipping and spin-conserving equation-of-motion coupled-cluster methods with single and double substitutions. *J. Chem. Phys.* **2008**, *129*, 194105.

(103) Casanova, D.; Slipchenko, L. V.; Krylov, A. I.; Head-Gordon, M. Double spin-flip approach within equation-of-motion coupled cluster and configuration interaction formalisms: Theory, implementation, and examples. *J. Chem. Phys.* **2009**, *130*, 044103.

(104) Dutta, A. K.; Pal, S.; Ghosh, D. Perturbative approximations to single and double spin flip equation of motion coupled cluster singles doubles methods. *J. Chem. Phys.* **2013**, *139*, 124116.

(105) Mato, J.; Gordon, M. S. A general spin-complete spin-flip configuration interaction method. *Phys. Chem. Chem. Phys.* **2018**, *20*, 2615−2626.

(106) Casanova, D.; Head-Gordon, M. Restricted active space spin-flip configuration interaction approach: theory, implementation and examples. *Phys. Chem. Chem. Phys.* **2009**, *11*, 9779−9790.

(107) Shao, Y.; Head-Gordon, M.; Krylov, A. I. The spin-flip approach within time-dependent density functional theory: Theory and applications to diradicals. *J. Chem. Phys.* **2003**, *118*, 4807−4818.

(108) Wang, F.; Ziegler, T. Time-Dependent Density Functional Theory Based on a Noncollinear Formulation of the Exchange-Correlation Potential. *J. Chem. Phys.* **2004**, *121*, 12191.

(109) Bernard, Y. A.; Shao, Y.; Krylov, A. I. General formulation of spin-flip time-dependent density functional theory using non-collinear kernels: Theory, implementation, and benchmarks. *J. Chem. Phys.* **2012**, *136*, 204103.

(110) Lefrancois, D.; Wormit, M.; Dreuw, A. Adapting algebraic diagrammatic construction schemes for the polarization propagator to problems with multi-reference electronic ground states exploiting the spin-flip ansatz. *J. Chem. Phys.* **2015**, *143*, 124107.

(111) Lefrancois, D.; Rehn, D. R.; Dreuw, A. Accurate adiabatic singlet-triplet gaps in atoms and molecules employing the third-order spin-flip algebraic diagrammatic construction scheme for the polarization propagator. *J. Chem. Phys.* **2016**, *145*, 084102.

(112) Mayhall, N. J.; Head-Gordon, M. Increasing spin-flips and decreasing cost: Perturbative corrections for external singles to the complete active space spin flip model for low-lying excited states and strong correlation. *J. Chem. Phys.* **2014**, *141*, 044112.

(113) Mayhall, N. J.; Goldey, M.; Head-Gordon, M. A Quasidegenerate Second-Order Perturbation Theory Approximation to RAS-nSF for Excited States and Strong Correlations. *J. Chem. Theory Comput.* **2014**, *10*, 589−599.

(114) Bell, F.; Zimmerman, P. M.; Casanova, D.; Goldey, M.; Head-Gordon, M. Restricted active space spin-flip (RAS-SF) with arbitrary number of spin-flips. *Phys. Chem. Chem. Phys.* **2013**, *15*, 358−366.

(115) Mayhall, N. J.; Horn, P. R.; Sundstrom, E. J.; Head-Gordon, M. Spin-flip non-orthogonal configuration interaction: a variational and almost black-box method for describing strongly correlated molecules. *Phys. Chem. Chem. Phys.* **2014**, *16*, 22694−22705.

(116) Golubeva, A. A.; Nemukhin, A. V.; Klippenstein, S. J.; Harding, L. B.; Krylov, A. I. Performance of the Spin-Flip and Multireference Methods for Bond Breaking in Hydrocarbons: A Benchmark Study. *J. Phys. Chem. A* **2007**, *111*, 13264−13271.

(117) Slipchenko, L. V.; Krylov, A. I. Singlet-triplet gaps in diradicals by the spin-flip approach: A benchmark study. *J. Chem. Phys.* **2002**, *117*, 4694−4708.

(118) Wang, T.; Krylov, A. I. The effect of substituents on electronic states' ordering in meta-xylylene diradicals: Qualitative insights from quantitative studies. *J. Chem. Phys.* **2005**, *123*, 104304.

(119) Slipchenko, L. V.; Krylov, A. I. Electronic structure of the trimethylenemethane diradical in its ground and electronically excited states: Bonding, equilibrium geometries, and vibrational frequencies. *J. Chem. Phys.* **2003**, *118*, 6874−6883.

(120) Rinkevicius, Z.; Ågren, H. Spin-flip time dependent density functional theory for singlet-triplet splittings in *sigma-sigma*-biradicals. *Chem. Phys. Lett.* **2010**, *491*, 132−135.

(121) Ibeji, C. U.; Ghosh, D. Singlet-triplet gaps in polyacenes: a delicate balance between dynamic and static correlations investigated by spin-flip methods. *Phys. Chem. Chem. Phys.* **2015**, *17*, 9849−9856.

(122) Hossain, E.; Deng, S. M.; Gozem, S.; Krylov, A. I.; Wang, X.-B.; Wenthold, P. G. Photoelectron Spectroscopy Study of Quinonimides. *J. Am. Chem. Soc.* **2017**, *139*, 11138−11148.

(123) Orms, N.; Rehn, D. R.; Dreuw, A.; Krylov, A. I. Characterizing Bonding Patterns in Diradicals and Triradicals by Density-Based Wave Function Analysis: A Uniform Approach. *J. Chem. Theory Comput.* **2018**, *14*, 638−648.

(124) Luxon, A. R.; Orms, N.; Kanters, R.; Krylov, A. I.; Parish, C. A. An ab Initio Exploration of the Bergman Cyclization. *J. Phys. Chem. A* **2018**, *122*, 420−430.

(125) Casanova, D. Avoided crossings, conical intersections, and low-lying excited states with a single reference method: The restricted active space spin-flip configuration interaction approach. *J. Chem. Phys.* **2012**, *137*, 084105.

(126) Gozem, S.; Krylov, A. I.; Olivucci, M. Conical Intersection and Potential Energy Surface Features of a Model Retinal Chromophore: Comparison of EOM-CC and Multireference Methods. *J. Chem. Theory Comput.* **2013**, *9*, 284−292.

(127) Nikiforov, A.; Gamez, J. A.; Thiel, W.; Huix-Rotllant, M.; Filatov, M. Assessment of approximate computational methods for conical intersections and branching plane vectors in organic molecules. *J. Chem. Phys.* **2014**, *141*, 124122.

(128) Strinati, G. Dynamical Shift and Broadening of Core Excitons in Semiconductors. *Phys. Rev. Lett.* **1982**, *49*, 1519.

(129) Rohlfing, M.; Louie, S. G. Electron-hole excitations and optical spectra from first principles. *Phys. Rev. B: Condens. Matter Mater. Phys.* **2000**, *62*, 4927−4944.

(130) Ma, Y.; Rohlfing, M.; Molteni, C. Excited states of biological chromophores studied using many-body perturbation theory: Effects of resonant-antiresonant coupling and dynamical screening. *Phys. Rev. B: Condens. Matter Mater. Phys.* **2009**, *80*, 241405.

(131) Ma, Y.; Rohlfing, M.; Molteni, C. Modeling the Excited States of Biological Chromophores within Many-Body Green's Function Theory. *J. Chem. Theory Comput.* **2010**, *6*, 257−265.

(132) Baumeier, B.; Andrienko, D.; Ma, Y.; Rohlfing, M. Excited States of Dicyanovinyl-Substituted Oligothiophenes from Many-Body Green's Functions Theory. *J. Chem. Theory Comput.* **2012**, *8*, 997−1002.

(133) Lettmann, T.; Rohlfing, M. Electronic Excitations of Polythiophene within Many-Body Perturbation Theory with and without the Tamm-Dancoff Approximation. *J. Chem. Theory Comput.* **2019**, *15*, 4547−4554.

(134) Hohenberg, P.; Kohn, W. Inhomogeneous electron gas. *Phys. Rev.* **1964**, *136*, B864−B871.

(135) Kohn, W.; Sham, L. J. Self-Consistent Equations Including Exchange and Correlation Effects. *Phys. Rev.* **1965**, *140*, A1133−A1138.

(136) Parr, R. G.; Yang, W. *Density-Functional Theory of Atoms and Molecules*; Clarendon Press: Oxford, U.K., 1989.

(137) Gill, P. M. W. Molecular Integrals Over Gaussian Basis Functions. *Adv. Quantum Chem.* **1994**, *25*, 141−205.

(138) Strinati, G.; Mattausch, H. J.; Hanke, W. Dynamical Correlation Effects on the Quasiparticle Bloch States of a Covalent Crystal. *Phys. Rev. Lett.* **1980**, *45*, 290−294.

(139) Hybertsen, M. S.; Louie, S. G. First-Principles Theory of Quasiparticles: Calculation of Band Gaps in Semiconductors and Insulators. *Phys. Rev. Lett.* **1985**, *55*, 1418−1421.

(140) Hybertsen, M. S.; Louie, S. G. Electron Correlation in Semiconductors and Insulators: Band Gaps and Quasiparticle Energies. *Phys. Rev. B: Condens. Matter Mater. Phys.* **1986**, *34*, 5390−5413.

(141) Godby, R. W.; Schlüter, M.; Sham, L. J. Self-Energy Operators and Exchange-Correlation Potentials in Semiconductors. *Phys. Rev. B: Condens. Matter Mater. Phys.* **1988**, *37*, 10159−10175.

(142) von der Linden, W.; Horsch, P. Precise Quasiparticle Energies and Hartree-Fock Bands of Semiconductors and Insulators. *Phys. Rev. B: Condens. Matter Mater. Phys.* **1988**, *37*, 8351−8362.

(143) Northrup, J. E.; Hybertsen, M. S.; Louie, S. G. Many-body Calculation of the Surface-State Energies for Si(111)2 × 1. *Phys. Rev. Lett.* **1991**, *66*, 500−503.

(144) Blase, X.; Zhu, X.; Louie, S. G. Self-Energy Effects on the Surface-State Energies of H-Si(111)1 × 1. *Phys. Rev. B: Condens. Matter Mater. Phys.* **1994**, *49*, 4973−4980.

(145) Rohlfing, M.; Krüger, P.; Pollmann, J. Efficient Scheme for GW Quasiparticle Band-Structure Calculations with Aapplications to Bulk Si and to the Si(001)-(2 × 1) Surface. *Phys. Rev. B: Condens. Matter Mater. Phys.* **1995**, *52*, 1905−1917.

(146) Shishkin, M.; Kresse, G. Self-Consistent GW Calculations for Semiconductors and Insulators. *Phys. Rev. B: Condens. Matter Mater. Phys.* **2007**, *75*, 235102.

(147) Loos, P. F.; Romaniello, P.; Berger, J. A. Green Functions and Self-Consistency: Insights From the Spherium Model. *J. Chem. Theory Comput.* **2018**, *14*, 3071−3082.

(148) Blase, X.; Attaccalite, C. Charge-Transfer Excitations in Molecular Donor-Acceptor Complexes within the Many-Body Bethe−Salpeter Approach. *Appl. Phys. Lett.* **2011**, *99*, 171909.

(149) Faber, C.; Attaccalite, C.; Olevano, V.; Runge, E.; Blase, X. First-Principles GW Calculations for DNA and RNA Nucleobases. *Phys. Rev. B: Condens. Matter Mater. Phys.* **2011**, *83*, 115123.

(150) Rangel, T.; Hamed, S. M.; Bruneval, F.; Neaton, J. B. Evaluating the GW Approximation with CCSD(T) for Charged Excitations Across the Oligoacenes. *J. Chem. Theory Comput.* **2016**, *12*, 2834−2842.

(151) Faleev, S. V.; van Schilfgaarde, M.; Kotani, T. All-Electron Self-Consistent G W Approximation: Application to Si, MnO, and NiO. *Phys. Rev. Lett.* **2004**, *93*, 126406.

(152) van Schilfgaarde, M.; Kotani, T.; Faleev, S. Quasiparticle Self-Consistent G W Theory. *Phys. Rev. Lett.* **2006**, *96*, 226402.

(153) Kotani, T.; van Schilfgaarde, M.; Faleev, S. V. Quasiparticle Self-Consistent G W Method: A Basis for the Independent-Particle Approximation. *Phys. Rev. B: Condens. Matter Mater. Phys.* **2007**, *76*, 165106.

(154) Ke, S.-H. All-Electron G W Methods Implemented in Molecular Orbital Space: Ionization Energy and Electron Affinity of Conjugated Molecules. *Phys. Rev. B: Condens. Matter Mater. Phys.* **2011**, *84*, 205415.

(155) Kaplan, F.; Harding, M. E.; Seiler, C.; Weigend, F.; Evers, F.; van Setten, M. J. Quasi-Particle Self-Consistent GW for Molecules. *J. Chem. Theory Comput.* **2016**, *12*, 2528−2541.

(156) Hanke, W.; Sham, L. J. Many-Particle Effects in the Optical Spectrum of a Semiconductor. *Phys. Rev. B: Condens. Matter Mater. Phys.* **1980**, *21*, 4656.

(157) Sottile, F.; Olevano, V.; Reining, L. Parameter-Free Calculation of Response Functions in Time-Dependent Density-Functional Theory. *Phys. Rev. Lett.* **2003**, *91*, 056402.

(158) Myöhänen, P.; Stan, A.; Stefanucci, G.; van Leeuwen, R. A many-body approach to quantum transport dynamics: Initial correlations and memory effects. *Europhys. Lett.* **2008**, *84*, 67001.

(159) Sakkinen, N.; Manninen, M.; van Leeuwen, R. The Kadanoff-Baym approach to double excitations in finite systems. *New J. Phys.* **2012**, *14*, 013032.

(160) Zhang, D.; Steinmann, S. N.; Yang, W. Dynamical second-order Bethe−Salpeter equation kernel: A method for electronic excitation beyond the adiabatic approximation. *J. Chem. Phys.* **2013**, *139*, 154109.

(161) Rebolini, E.; Toulouse, J. Range-separated time-dependent density-functional theory with a frequency-dependent second-order Bethe−Salpeter correlation kernel. *J. Chem. Phys.* **2016**, *144*, 094107.

(162) Olevano, V.; Toulouse, J.; Schuck, P. A formally exact one-frequency-only Bethe−Salpeter-like equation. Similarities and differ-

ences between GW+BSE and self-consistent RPA. *J. Chem. Phys.* **2019**, *150*, 084112.

(163) Casida, M. E.; Huix-Rotllant, M. Many-Body Perturbation Theory (MBPT) and Time-Dependent Density-Functional Theory (TD-DFT): MBPT Insights About What Is Missing In, and Corrections To, the TD-DFT Adiabatic Approximation. *Top. Curr. Chem.* **2015**, *368*, 1−60.

(164) Harbach, P. H. P.; Wormit, M.; Dreuw, A. The Third-Order Algebraic Diagrammatic Construction Method (ADC(3)) for the Polarization Propagator for Closed-Shell Molecules: Efficient Implementation and Benchmarking. *J. Chem. Phys.* **2014**, *141*, 064113.

(165) Kánnár, D.; Szalay, P. G. Benchmarking Coupled Cluster Methods on Valence Singlet Excited States. *J. Chem. Theory Comput.* **2014**, *10*, 3757−3765.

(166) Chrayteh, A.; Blondel, A.; Loos, P.-F.; Jacquemin, D. Mountaineering Strategy to Excited States: Highly Accurate Oscillator Strengths and Dipole Moments of Small Molecules. *J. Chem. Theory Comput.* **2021**, *17*, 416.

(167) Sarkar, R.; Boggio-Pasqua, M.; Loos, P. F.; Jacquemin, D. Benchmark of TD-DFT and Wavefunction Methods for Oscillator Strengths and Excited-State Dipole Moments. *J. Chem. Theory Comput.* **2021**, *17*, 1117−1132.

(168) Véril, M.; Romaniello, P.; Berger, J. A.; Loos, P. F. Unphysical Discontinuities in GW Methods. *J. Chem. Theory Comput.* **2018**, *14*, 5220.

(169) Berger, J. A.; Loos, P.-F.; Romaniello, P. Potential energy surfaces without unphysical discontinuities: the Coulomb-hole plus screened exchange approach. *J. Chem. Theory Comput.* **2021**, *17*, 191.

(170) Loos, P. F.; Pradines, B.; Scemama, A.; Giner, E.; Toulouse, J. A Density-Based Basis-Set Incompleteness Correction for GW Methods. *J. Chem. Theory Comput.* **2020**, *16*, 1018−1028.

(171) Stein, T.; Kronik, L.; Baer, R. Reliable Prediction of Charge Transfer Excitations in Molecular Complexes Using Time-Dependent Density Functional Theory. *J. Am. Chem. Soc.* **2009**, *131*, 2818−2820.

(172) Stein, T.; Eisenberg, H.; Kronik, L.; Baer, R. Fundamental Gaps in Finite Systems from Eigenvalues of a Generalized Kohn-Sham Method. *Phys. Rev. Lett.* **2010**, *105*, 266802.

(173) Refaely-Abramson, S.; Sharifzadeh, S.; Govind, N.; Autschbach, J.; Neaton, J. B.; Baer, R.; Kronik, L. Quasiparticle Spectra from a Nonempirical Optimally Tuned Range-Separated Hybrid Density Functional. *Phys. Rev. Lett.* **2012**, *109*, 226405.

(174) Kronik, L.; Stein, T.; Refaely-Abramson, S.; Baer, R. Excitation Gaps of Finite-Sized Systems from Optimally Tuned Range-Separated Hybrid Functionals. *J. Chem. Theory Comput.* **2012**, *8*, 1515−1531.

(175) Loos, P. F. *QuAcK: a software for emerging quantum electronic structure methods*. 2019; https://github.com/pfloos/QuAcK.

(176) Shao, Y.; et al. Advances in Molecular Quantum Chemistry Contained in the Q-Chem 4 Program Package. *Mol. Phys.* **2015**, *113*, 184−215.

(177) Becke, A. D. Density-functional exchange-energy approximation with correct asymptotic behavior. *Phys. Rev. A: At., Mol., Opt. Phys.* **1988**, *38*, 3098.

(178) Lee, C.; Yang, W.; Parr, R. G. Development of the Colle-Salvetti correlation-energy formula into a functional of the electron density. *Phys. Rev. B: Condens. Matter Mater. Phys.* **1988**, *37*, 785.

(179) Becke, A. D. Density-Functional Thermochemistry. III. The Role of Exact Exchange. *J. Chem. Phys.* **1993**, *98*, 5648−5652.

(180) Becke, A. D. A new mixing of Hartree-Fock and local density-functional theories. *J. Chem. Phys.* **1993**, *98*, 1372−1377.

(181) Yanai, T.; Tew, D. P.; Handy, N. C. A New Hybrid Exchange-Correlation Functional Using the Coulomb-Attenuating Method (CAM-B3LYP). *Chem. Phys. Lett.* **2004**, *393*, 51−57.

(182) Weintraub, E.; Henderson, T. M.; Scuseria, G. E. Long-Range-Corrected Hybrids Based on a New Model Exchange Hole. *J. Chem. Theory Comput.* **2009**, *5*, 754−762.

(183) Chai, J. D.; Head-Gordon, M. Systematic Optimization of Long-Range Corrected Hybrid Density Functionals. *J. Chem. Phys.* **2008**, *128*, 084106.

(184) Chai, J. D.; Head-Gordon, M. Long-range Corrected Hybrid Density Functionals with Damped Atom-Atom Dispersion Corrections. *Phys. Chem. Chem. Phys.* **2008**, *10*, 6615−6620.

(185) Koch, H.; Jensen, H. J. A.; Jorgensen, P.; Helgaker, T. Excitation Energies from the Coupled Cluster Singles and Doubles Linear Response Function (CCSDLR). Applications to Be, CH $^+$, CO, and H $_2$ O. *J. Chem. Phys.* **1990**, *93*, 3345−3350.

(186) Stanton, J. F.; Bartlett, R. J. The equation of motion coupled-cluster method. A systematic biorthogonal approach to molecular excitation energies, transition probabilities, and excited state properties. *J. Chem. Phys.* **1993**, *98*, 7029−7039.

(187) Koch, H.; Kobayashi, R.; Sanchez de Merás, A.; Jorgensen, P. Calculation of size-intensive transition moments from the coupled cluster singles and doubles linear response function. *J. Chem. Phys.* **1994**, *100*, 4393−4400.

(188) Frisch, M. J. et al. *Gaussian 09*, Rev. E.01; Gaussian Inc.: Wallingford, CT, 2009.

(189) Caruso, F.; Rohr, D. R.; Hellgren, M.; Ren, X.; Rinke, P.; Rubio, A.; Scheffler, M. Bond Breaking and Bond Formation: How Electron Correlation Is Captured in Many-Body Perturbation Theory and Density-Functional Theory. *Phys. Rev. Lett.* **2013**, *110*, 146403.

(190) Barca, G. M. J.; Gilbert, A. T. B.; Gill, P. M. W. Hartree-Fock description of excited states of H2. *J. Chem. Phys.* **2014**, *141*, 111104.

(191) Vuckovic, S.; Gori-Giorgi, P. Simple Fully Nonlocal Density Functionals for Electronic Repulsion Energy. *J. Phys. Chem. Lett.* **2017**, *8*, 2799−2805.

(192) Li, J.; Olevano, V. Hydrogen-molecule spectrum by the many-body GW approximation and the Bethe−Salpeter equation. *Phys. Rev. A: At., Mol., Opt. Phys.* **2021**, *103*, 012809.

(193) Cohen, A. J.; Mori-Sánchez, P.; Yang, W. Fractional Spins and Static Correlation Error in Density Functional Theory. *J. Chem. Phys.* **2008**, *129*, 121104.

(194) Cohen, A. J.; Mori-Sánchez, P.; Yang, W. Insights into Current Limitations of Density Functional Theory. *Science* **2008**, *321*, 792−794.

(195) Cohen, A. J.; Mori-Sánchez, P.; Yang, W. Challenges for Density Functional Theory. *Chem. Rev.* **2012**, *112*, 289−320.

(196) Coulson, C.; Fischer, I. XXXIV. Notes on the Molecular Orbital Treatment of the Hydrogen Molecule. *Philos. Mag.* **1949**, *40*, 386.

(197) Balková, A.; Bartlett, R. J. A multireference coupled-cluster study of the ground state and lowest excited states of cyclobutadiene. *J. Chem. Phys.* **1994**, *101*, 8972−8987.

(198) Karadakov, P. B. Ground- and Excited-State Aromaticity and Antiaromaticity in Benzene and Cyclobutadiene. *J. Phys. Chem. A* **2008**, *112*, 7303−7309.

(199) Li, X.; Paldus, J. Accounting for the exact degeneracy and quasidegeneracy in the automerization of cyclobutadiene via multi-reference coupled-cluster methods. *J. Chem. Phys.* **2009**, *131*, 114103.

(200) Shen, J.; Piecuch, P. Combining active-space coupled-cluster methods with moment energy corrections via the CC(P;Q) methodology, with benchmark calculations for biradical transition states. *J. Chem. Phys.* **2012**, *136*, 144104.

(201) Vitale, E.; Alavi, A.; Kats, D. FCIQMC-Tailored Distinguishable Cluster Approach. *J. Chem. Theory Comput.* **2020**, *16*, 5621−5634.

(202) Head-Gordon, M.; Rico, R. J.; Oumi, M.; Lee, T. J. A Doubles Correction To Electronic Excited States From Configuration Interaction In The Space Of Single Substitutions. *Chem. Phys. Lett.* **1994**, *219*, 21−29.

(203) Head-Gordon, M.; Maurice, D.; Oumi, M. A Perturbative Correction to Restricted Open-Shell Configuration-Interaction with Single Substitutions for Excited-States of Radicals. *Chem. Phys. Lett.* **1995**, *246*, 114−121.

(204) Trofimov, A.; Schirmer, J. Polarization Propagator Study of Electronic Excitation in key Heterocyclic Molecules I. Pyrrole. *Chem. Phys.* **1997**, *214*, 153−170.

(205) Dreuw, A.; Wormit, M. The Algebraic Diagrammatic Construction Scheme for the Polarization Propagator for the Calculation of Excited States. *Wiley Interdiscip. Rev. Comput. Mol. Sci.* **2015**, *5*, 82−95.

(206) Christiansen, O.; Koch, H.; Jørgensen, P. The Second-Order Approximate Coupled Cluster Singles and Doubles Model CC2. *Chem. Phys. Lett.* **1995**, *243*, 409−418.

(207) Trofimov, A. B.; Stelter, G.; Schirmer, J. Electron Excitation Energies Using a Consistent Third-Order Propagator Approach: Comparison with Full Configuration Interaction and Coupled Cluster Results. *J. Chem. Phys.* **2002**, *117*, 6402−6410.